UCLA

UCLA Previously Published Works

Title

An improved dust emission model – Part 2: Evaluation in the Community Earth System Model, with implications for the use of dust source functions

Permalink

https://escholarship.org/uc/item/632300dg

Journal

Atmospheric Chemistry and Physics, 14(23)

ISSN

1680-7316

Authors

Kok, JF
Albani, S
Mahowald, NM
et al.

Publication Date

2014

DOI

10.5194/acp-14-13043-2014

Peer reviewed

An improved dust emission model. Part 2: Evaluation in the Community Earth System Model, with implications for the use of dust source functions

Kok, J. F.[1], S. Albani[2], N. M. Mahowald[2], and D. S. Ward[2]

[1] Department of Atmospheric and Oceanic Sciences, University of California, Los Angeles, CA 90095, USA
[2] Department of Earth and Atmospheric Sciences, Cornell University, Ithaca, NY 14850, USA

Correspondence to J. F. Kok (jfkok@ucla.edu)

Abstract

The complex nature of mineral dust aerosol emission makes it a difficult process to represent accurately in weather and climate models. Indeed, both measurements and the new physically-based dust emission parameterization presented in the companion paper indicate that many large-scale models underestimate the dust flux's sensitivity to the soil's threshold friction velocity. We hypothesize that this finding explains why many dust cycle simulations are improved by using an empirical dust source function that shifts emissions towards the world's most erodible regions. Here, we both test this hypothesis and evaluate the performance of the new dust emission parameterization. We do so by implementing the new emission scheme into the Community Earth System Model (CESM) and comparing the resulting dust cycle simulations against an array of measurements. We find that the new scheme shifts emissions towards the world's most erodible regions in a manner that is strikingly similar to the effect of implementing a widely-used source function based on satellite observations by the Total Ozone Mapping Spectrometer. Furthermore, model comparisons against aerosol optical depth measurements show that the new physically-based scheme produces a statistically significant improvement in CESM's representation of dust emission, which exceeds the improvement produced by implementing a source function. These results indicate that the need to use an empirical source function is (partially) eliminated, at least in CESM, by the additional physics in the new scheme, and in particular by its increased sensitivity to the soil's threshold friction velocity. Since the threshold friction velocity is affected by climate changes, our results further suggest that many large-scale models underestimate the global dust cycle's climate sensitivity.

-

1. Introduction

Mineral dust aerosols affect the Earth system through a wide variety of interactions, including scattering and absorbing radiation, altering cloud lifetime and reflectance, and serving as a nutrient source (Martin et al., 1991; Miller and Tegen, 1998; Forster et al., 2007). Conversely, the global dust cycle is highly sensitive to changes in climate (Tegen et al., 2004; Mahowald et al., 2006b; Washington et al., 2009), as evidenced both by global dust deposition being several times larger during glacial maxima than during interglacials (Rea, 1994; Harrison et al., 2001) and by the apparent increase in global dust deposition over the past century (Prospero and Lamb, 2003; Mahowald et al., 2010). The radiative forcing resulting from such changes in the dust cycle might have played a critical role in amplifying past climate changes (Jansen et al., 2007), and may play an important role in present and future climate changes (Harrison et al., 2001; Mahowald et al., 2010).

Unfortunately, an accurate quantification of dust interactions with the Earth system in past and future climates is hindered by the empirical nature of dust emission parameterizations in climate models. Since these parameterizations are generally tuned to reproduce the current dust cycle (Ginoux et al., 2001; Zender et al., 2003a; Cakmur et al., 2006), applying them to a past or future climate, with substantial differences in global circulation and land surface, could produce large systematic errors. In particular, many dust modules in climate models use a *dust source function S* (Ginoux et al., 2001; Tegen et al., 2002; Zender et al., 2003b; Grini et al., 2005; Koven and Fung, 2008) to help account for global variations in *soil erodibility* (defined in the dust modeling community as the efficiency of a soil in producing dust aerosols under a given wind stress (Zender et al., 2003b)).

The flux of dust emitted through wind erosion in a model grid cell is thus commonly represented by (Ginoux et al., 2001; Zender et al., 2003a; Grini et al., 2005; Colarco et al., 2014)

$$\phi_d = C_{\text{tune}} S F_d \qquad \qquad ()$$

,

where C_{tune} is a global tuning constant, usually set to maximize agreement against observations (Cakmur et al., 2006), and F_d is the vertical dust flux produced by an eroding soil per unit time and area, as predicted by a dust emission parameterization such as Gillette and Passi (1988), Marticorena and Bergametti (1995), or Kok et al. (2014). The dust source function S is a function of latitude and longitude, and usually shifts emissions towards the world's most erodible regions, such as North Africa (Ginoux et al., 2001; Tegen et al., 2002; Zender et al., 2003b).

The need to use a source function to improve agreement against observations was first noted by the pivotal study of Ginoux et al. (2001). They used the observation of Prospero et al. (2002) that dust "hot spots" tend to be co-located with topographic depressions to design a source function based on the relative height of a model grid cell compared to its surrounding cells. However, some subsequent studies challenged this association of dust hot spots with topographic depressions by Prospero et al. (2002) because (i) the used remote sensing product from the Total Ozone Mapping Spectrometer (TOMS) is sensitive to boundary layer height, which tends to be higher over depressions in central desert regions (Mahowald and Dufresne, 2004), and because (ii) advection causes the remotely sensed dust loading to be shifted downwind from source regions (Schepanski et al., 2009). Nonetheless, the use of source functions, and the consequent shift of emissions towards regions with observed high dust loadings (Ginoux et al., 2001;

75 Prospero et al., 2002), can substantially improve the agreement of dust cycle simulations with
76 measurements (Zender et al., 2003b; Cakmur et al., 2006).
77   This improvement of dust cycle simulations by semi-empirical source functions suggests that
78 a key piece of physics is missing from existing dust emission parameterizations in models. And
79 indeed, dust flux parameterizations in most large-scale models account for variations in soil
80 erodibility in mostly empirical manners. The dust emission parameterization of Gillette and Passi
81 (1988), which is used in the Goddard Chemistry Aerosol Radiation and Transport (GOCART)
82 model (Ginoux et al., 2001) and many other models (Huneeus et al., 2011), does not account for
83 the effect of either sediment availability or other soil properties on the dust flux. Similarly, the
84 dust flux parameterization of Marticorena and Bergametti (1995), which is used in simplified
85 form in the Dust Entrainment And Deposition model (Zender et al., 2003a) that is used in many
86 climate models (Huneeus et al., 2011), accounts for the effect of fine sediment availability on the
87 dust flux using an empirical fit to data from a single study (Gillette, 1979). Since such empirical
88 parameterizations and source functions cannot accurately capture changes in soil erodibility
89 produced by climate changes, which for instance affect soil moisture content and soil
90 aggregation (Zobeck, 1991; Fecan et al., 1999; Shao, 2008; Kok et al., 2012), their use could
91 cause substantial errors in model estimates of climate-induced changes in the global dust cycle.
92   This paper and its companion paper (Kok et al., 2014) strive to take a step towards an
93 improved representation of the global dust cycle in climate models, in particular for climate
94 regimes other than the current climate to which most models are tuned (Cakmur et al., 2006).
95 The first component of this objective was achieved in our companion paper (Kok et al., 2014),
96 by presenting a physically-based theory for the vertical dust flux emitted by an eroding soil. The resulting
97 parameterization (henceforth referred to as K14) was able to reproduce a quality-controlled
98 compilation of dust flux measurements with substantially less error than the existing dust flux
99 parameterizations we were able to test against, and is relatively straightforward to implement since it
100 uses only globally-available parameters. A critical insight from our companion paper is that the dust flux
101 is likely substantially more sensitive to changes in the soil state than most climate models account for.
102 The resulting underestimation of the dust flux sensitivity to the soil state might explain why an empirical
103 source function that shifts emissions towards more erodible regions improves agreement against
104 measurements (Cakmur et al., 2006). Since the new K14 scheme accounts for the increased sensitivity of
105 the dust flux to the soil state, our companion paper hypothesized that K14 can reduce the need to use a
106 source function in dust cycle simulations.
107   Here we use simulations with the Community Earth System Model (CESM) to both test the
108 above hypothesis, and to evaluate the performance of the K14 parameterization in a climate model.
109 Through a detailed comparison against measurements, we find that the K14 scheme produces a
110 statistically significant improvement in the representation of dust emission in CESM, and that this
111 improvement exceeds that produced by a source function. These results indicate that the additional
112 physics accounted for by K14, which result in an increased sensitivity of the dust flux to the soil's
113 threshold friction velocity, reduces the need for a source function in dust cycle simulations, at least in
114 CESM. Since the threshold friction velocity is affected by climate changes, our finding that many
115 models underestimate the dust flux's sensitivity to this threshold further suggests that these
116 models have underestimated the global dust cycle's climate sensitivity.
117   The next section describes CESM's dust module and the implementation of the K14 dust
118 emission parameterization, as well as the measurements used to evaluate the fidelity of CESM's
119 dust cycle simulations. We then present results of the comparison between simulations and
120 measurements in Section 3, discuss the implications of the results in Section 4, and summarize
121 and conclude the paper in Section 5.

3

122

2. Methods

124 We use simulations with CESM version 1.1 (Hurrell et al., 2013) to evaluate the performance of
125 the K14 dust emission scheme. Specifically, we simulate the present-day dust cycle with four
126 different combinations of source functions and dust flux parameterizations (see Table 1). In order
127 to assess whether K14 improves the representation of dust emission in CESM, we compare the
128 simulation results against measurements of aerosol optical depth (AOD) by the AERosol
129 RObotic NETwork (AERONET; Holben et al. (1998)), as well as to satellite-derived estimates of
130 dust optical depth and dust mass path close to source regions (Evan et al., 2014). Note that the
131 code to implement the K14 parameterization in CESM is freely available from the main author.
132 　　We also evaluate how each of the four dust cycle simulations performs against measurements
133 further from source regions, namely dust surface concentration and dust deposition. Since these
134 measurements were thus generally taken far from source regions, the simulation performance
135 against these measurements depends on the model's ability to simulate a variety of other
136 processes in addition to dust emission, especially transport and deposition.
137 　　The next section briefly describes CESM and its treatment of the dust cycle for each of the
138 four simulations (Table 1). We then describe the properties of the data sets used to evaluate the
139 model performance in Sections 2.2 and 2.3. In Section 2.4, we describe the method to assess
140 whether improvements in the ability of the different simulations to reproduce these
141 measurements are statistically significant.

142

143 **Table 1.** Summary of the four CESM simulations used in this study, and the statistics of their
144 comparison against the data set most characteristic of dust emission, namely AERONET AOD
145 measurements at dusty stations (see text). Model results are compared to measurements of
146 AERONET AOD climatology (fourth and fifth columns), the mean correlation to the measured
147 seasonal cycle at each station (sixth column), and the mean correlation to the measured daily
148 variability at each station (seventh column). Statistically significant improvements (see Section
149 2.4) of Simulations II-IV relative to the 'control' Simulation I are indicated with bold font.
150 Additionally, simulation results that are statistically significantly improved over the results of
151 each of the other three simulations are both bold and underlined.

Simulation	Dust flux parameterization	Dust source function	AERONET climatology, r	AERONET climatology, RMSE	AERONET seasonal cycle, r	AERONET daily variability, r
I	Zender et al. (2003a)	None	0.55	0.149	0.79	0.43
II	Zender et al. (2003a)	Zender et al. (2003b)	0.57	0.146	0.75	0.43
III	Zender et al. (2003a)	Ginoux et al. (2001)	0.62	0.138	0.79	0.42
IV	Kok et al. (2014)	None	**0.72**	**0.117**	**0.82**	**0.46**

152

2.1. Dust cycle simulations with the Community Earth System Model

154 Emission of dust aerosols in CESM was calculated using its land model, the Community Land
155 Model version 4.0 (CLM4, Lawrence et al. (2011)). These emissions were then used by CESM's

4

156 atmosphere model, the Community Atmosphere Model version 4 (CAM4), to calculate the three-
157 dimensional transport and deposition of dust, as well as the dust aerosol optical depth
158 (Mahowald et al., 2006b; Albani et al., 2014). In addition to accounting for the global dust cycle
159 and the consequent optical depth produced by dust aerosols (see next section), CESM also
160 includes the effects of other kinds of aerosols, including sea salt, biomass burning, and sulfate
161 aerosols. Black and organic carbon, dimethyl-sulphide, and sulphur oxides emissions are
162 prescribed based on AeroCom specifications (Neale et al., 2010), whereas sea salt aerosol
163 emission is prognostic, based on 10 m wind speed and humidity (Mahowald et al., 2006a).
164

165 2.1.1. General treatment of the dust cycle in CESM

166 The emission of dust aerosols in CLM4 follows the treatment of Zender et al. (2003a), with
167 modifications described in Mahowald et al. (2006b, 2010), and further adjustments described

$$\phi_d$$

168 below. Specifically, the vertical dust flux   in a model grid cell is parameterized using Eq. (1),
169 with the source function S and the vertical dust flux F_d given in Table 1 for the four simulations
170 (also see 2.1.2). We adjust the global tuning factor C_{tune} to maximize agreement against
171 AERONET AOD measurements (see Section 2.1.2).
172   The threshold friction velocity u_{*t}' at which dust emission is initiated is critical to
173 determining dust emissions. The value of u_{*t}' depends on air density, soil properties, and the
174 presence of non-erodible roughness elements (Marticorena and Bergametti, 1995; Shao and Lu,
175 2000; Kok et al., 2014). However, CLM4 does not account for the effect of non-erodible
176 roughness elements on dust emissions, and the effect of air density on u_{*t}' is limited.
177 Consequently, u_{*t}' in CLM4 is mostly determined by soil moisture content; the treatment of the
178 effect of soil moisture on u_{*t}' follows Eqs. (12) and (14) in Fécan et al. (1999):

$$\frac{u_{*t}'}{u_{*dt}'} = 1, \qquad\qquad\qquad\qquad ()$$

$$(w < w')$$

$$\frac{u_{*t}'}{u_{*dt}'} = \sqrt{1+1.21(w-w')^{0.68}} \qquad\qquad ()$$

$$(w \geq w'),$$

179 where u_{*t}' and u_{*dt}' are respectively the threshold friction velocities in the presence and absence
180 of soil moisture, and u_{*dt}' is calculated following the semi-empirical relation of Iversen and White
181 (1982), as described on p. 3 of Zender et al. (2003a). Furthermore, w is the gravimetric water
182 content in percent for CLM4's top soil layer, which has a thickness of 1.75 cm (Oleson et al.,
183 2010). The threshold gravimetric water content w' of the top soil layer above which w increases
184 u_{*t}' is given by (Fecan et al., 1999; Zender et al., 2003a)

$$w' = b\left(17 f_{clay} + 14 f_{clay}^2\right) \qquad\qquad ()$$

,

185 where w' is given in percent, b is a tuning parameter introduced by Zender et al. (2003a), and
186 f_{clay} is the soil's clay fraction, which is taken from the FAO (2012) soil database (see Fig. S1).
187   The larger the value of the tuning parameter b, the smaller the effect of soil moisture on the
188 dust emission threshold u_{*t}'. The range of plausible values of b extends from less than 1, to 1
189 (i.e., no tuning constant; Fecan et al. (1999)) to 3 (Mokhtari et al., 2012) to 1/f_{clay} (Zender et al.,

190 [2003a](). Since dust emissions are non-linear in $u_{*\mathrm{t}}$' (e.g., [Kok et al. (2014)]()), and since $u_{*\mathrm{t}}$' is a
191 critical variable in the K14 dust emission scheme tested in this paper, the choice of b can be
192 expected to substantially affect the simulated dust cycle. Unfortunately, the 'correct' value of b is
193 highly uncertain, in part because the parameterization of Fecan et al. (1999) is based on wind
194 tunnel studies. Implementing this small-scale parameterization into a climate model scales it up
195 by many orders of magnitude, potentially producing physically unrealistic results. Furthermore,
196 the inhibition of dust emission by soil moisture depends on the moisture content of the top layer
197 of soil particles ([McKenna Neuman and Nickling, 1989]()), which is in direct contact with the
198 surface air. In contrast, the top soil layer of hydrology models in climate models usually has a
199 thickness of multiple centimeters and thus responds differently to precipitation and changes in
200 atmospheric humidity, which are important in determining the dust emission threshold ([Ravi et
201 al., 2004](); [Ravi et al., 2006]()). The 'correct' value of b in a climate model is therefore likely to
202 depend substantially on the model methodology, and in particular on the specifics of the model's
203 hydrology module. Since the choice of b is thus ambiguous, we investigated the sensitivity of our
204 results to the particular value of b by running simulations with a wide range of values (Table S1).
205 We emphasize that other models using the K14 scheme should do a similar sensitivity study to
206 avoid an unrealistic influence of the model's hydrology on the dust emission fluxes. Because we
207 found that the simplest case of not using a tuning constant (i.e., $b = 1$) produces the best overall
208 results for all four model configurations, we used $b = 1$ for the results reported in Section 3. But
209 note that the wide range of values of b that we tested all produced results qualitatively similar to
210 those presented here (see Table S1).
211   In addition to the effects of soil moisture, CLM4 also accounts for the inhibition of dust
212 emissions by vegetation. Specifically, CLM4 assumes that the fraction of the grid cell consisting
213 of bare soil capable of emitting dust aerosols (f_{bare}) decreases linearly with the leaf area index
214 (LAI), which is the ratio of the total surface area of leaves with the land surface area. That is,

$$f_{\mathrm{bare}} = 1 - \lambda / \lambda_{\mathrm{thr}} \qquad\qquad\qquad\qquad\qquad ()$$
$$, \qquad\qquad (\lambda \le \lambda_{\mathrm{thr}})$$

215 where λ denotes LAI, and $\lambda_{\mathrm{thr}} = 0.3$ is the threshold LAI above which no dust emission is
216 assumed to occur ([Mahowald et al., 2010]()). (Note that the [Ginoux et al. (2001)]() source function
217 already includes the effects of vegetation, such that f_{bare} is set to 1 for all grid cells in Simulation
218 III (see Table 1) to prevent accounting for the effects of vegetation twice.)
219   After CLM4 has calculated the dust flux, CAM4 distributes the emitted dust aerosols into 4
220 size bins ([Mahowald et al., 2006b]()), from $0.1 – 1.0$ µm, $1.0 – 2.5$ µm, $2.5 – 5.0$ µm, and $5.0 – 10$
221 µm. The fraction distributed into each bin follows the 'brittle fragmentation' dust size
222 distribution derived in [Kok (2011b)](), which is in good agreement with a wide range of
223 measurements ([Mahowald et al., 2014]()). The emitted dust size distribution does not depend on the
224 wind speed at emission, as shown by measurements ([Kok, 2011a]()). The optical properties for
225 each bin are specified in [Albani et al. (2014)]() and are derived from a representation of dust as an
226 internal mixture of the primary mineral classes of dust (quartz, aluminosilicates, clays,
227 carbonates, iron-bearing minerals), combined into an effective medium using the Maxwell
228 Garnett approximation (e.g., [Videen and Chylek (1998)]()). The proportions of the mineral classes
229 are consistent with the ranges reported in atmospheric dust and its parent soils ([Claquin et al.,
230 1999]()), and they are in agreement with bulk optical properties observed in dusty regions ([Albani
231 et al., 2014]()). The resulting radiative effects of dust aerosols do not feed back onto the simulated
232 atmospheric dynamics.

233   CAM4 simulates both dry and wet deposition of dust. Dry deposition includes turbulent and
234 gravitational settling, and follows the treatment in Zender et al. (2003a). Wet deposition accounts
235 for in- and below-cloud scavenging and follows Neale et al. (2010) with the modifications
236 described in Albani et al. (2014), which improve the model's ability to simulate the observed
237 spatial gradients of dust. Specifically, the dust solubility (i.e., the fraction of dust available for in-
238 cloud removal) was changed from 0.15 to 0.30, in line with a more recent version of the model
239 (Liu et al., 2012). In addition, instead of using a constant below-cloud scavenging coefficient
240 (collection efficiency) of 0.1 (Balkanski et al., 1993; Neale et al., 2010), the scavenging
241 coefficient was made size-dependent (Andronache, 2003; Zender et al., 2003a), and was set to
242 0.1 for dust diameters below 2.5 µm and 0.3 for larger dust particles.
243

2.1.2. Dust emission schemes of the four CESM simulations

245 We used CESM to conduct four simulations, each with a different dust emission scheme (Table
246 1). The 'control' Simulation I uses CESM's default dust emission parameterization of Zender et
247 al. (2003a) (henceforth referred to as Z03) and does not use a source function; Simulations II and
248 III then respectively add the source functions of Zender et al. (2003b) and Ginoux et al. (2001);
249 and Simulation IV replaces the Zender et al. (2003a) parameterization with the K14
250 parameterization and also does not use a source function.
251   For Simulations I – III, F_d thus follows Z03, which is essentially a simplified version of the
252 Marticorena and Bergametti (1995) parameterization. It is given by

$$F_\mathrm{d} = C_\mathrm{MB}\eta f_\mathrm{bare} \frac{\rho_\mathrm{a}}{g} u_*'^3 \left(1 - \frac{u_{*\mathrm{t}}'^2}{u_*'^2}\right)\left(1 + \frac{u_{*\mathrm{t}}'}{u_*'}\right) \qquad \left(u_*' > u_{*\mathrm{t}}'\right) \tag{6}$$
, ,

253 where C_MB is a dimensionless proportionality constant, ρ_a is the air density, g is the gravitational
254 acceleration, and the sandblasting efficiency η (units of m^{-1}) depends on the soil clay fraction f_clay

$$\eta = 10^{13.4 f_\mathrm{clay} - 6}$$

255 (see Fig. S1) following   . Note that, whereas the soil friction velocity u_* is defined
256 from the wind stress on the bare erodible soil, the friction velocity u_*' is defined by the wind
257 stress on the entire surface, so including the stress on non-erodible roughness elements (see Kok
258 et al. (2014) for exact definitions). But since Z03 (and thus CLM4) does not account for the
259 presence of non-erodible roughness elements, we have that $u_* = u_*'$, and $u_{*\mathrm{t}} = u_{*\mathrm{t}}'$, where $u_{*\mathrm{t}}$ and
260 $u_{*\mathrm{t}}'$ are respectively the threshold friction velocity and the threshold soil friction velocity above
261 which dust emissions occur.
262   Simulation IV uses the K14 dust emission parameterization (Kok et al., 2014), which is given
263 by

$$F_\mathrm{d} = C_\mathrm{d} f_\mathrm{bare} f_\mathrm{clay} \frac{\rho_\mathrm{a}\left(u_*^2 - u_{*\mathrm{t}}^2\right)}{u_{*\mathrm{st}}} \left(\frac{u_*}{u_{*\mathrm{t}}}\right)^{C_\alpha \frac{u_{*\mathrm{st}} - u_{*\mathrm{st}0}}{u_{*\mathrm{st}0}}} \qquad \left(u_* > u_{*\mathrm{t}}\right) \tag{7a}$$
, .

264 The standardized threshold friction velocity $u_{*\mathrm{st}}$ is the value of $u_{*\mathrm{t}}$ at standard atmospheric density

$$u_{*\mathrm{st}} \equiv u_{*\mathrm{t}} \sqrt{\rho_\mathrm{a} / \rho_\mathrm{a0}}$$

265 (ρ_a0 = 1.225 kg/m^3), that is,   . $u_{*\mathrm{st}0}$ is then the minimal value of $u_{*\mathrm{st}}$ for an

266 optimally-erodible soil, and measurements show that $u_{*st0} \approx 0.16$ m/s (Kok et al., 2012).
267 Furthermore, the dust emission coefficient C_d is a measure of soil erodibility (i.e., a soil's ability
268 to produce dust) that depends only on the standardized threshold friction velocity, and is defined
269 as

$$C_d = C_{d0} \exp\left(-C_e \frac{u_{*st} - u_{*st0}}{u_{*st0}} \right) \tag{7b}$$

.

270 The dimensionless coefficients in Eq. (7) were determined in Kok et al. (2014) from comparison
271 against a quality-controlled compilation of dust flux measurements, and are as follows: $C_\alpha = 2.7$
272 ± 1.0, $C_e = 2.0 \pm 0.3$ and $C_{d0} = (4.4 \pm 0.5) \times 10^{-5}$.
273   As discussed in Kok et al. (2014), Eq. (7) accounts for the experimental observation that a
274 more erodible soil produces a larger flux of dust per saltator impact. That is, per Eq. (7b), the
275 dust flux F_d increases exponentially with a decrease in the standardized threshold u_{*st}.
276 Consequently, the dust flux is substantially more sensitive to the soil's threshold friction velocity
277 in K14 than in Z03 (Fig. 1), which is in agreement with measurements (Kok et al., 2014). We
278 discuss the implications of the increased sensitivity of the dust flux to the threshold friction
279 velocity in Sections 4.2 and 4.3.
280   The simulations used the capability of CESM to be forced with reanalysis winds instead of
281 predicting winds, and used the ERA-Interim reanalysis meteorology from the European Centre
282 for Medium-range Weather Forecasts (ECMWF) (Dee et al., 2011; Ma et al., 2013). CESM uses
283 Monin-Obukhov Similarity Theory to obtain the friction velocity u_*' from the wind field (see
284 section 5.1 in Oleson et al. (2010)). All simulations were run at a resolution of 1.9° latitude by
285 2.5° longitude, and cover the period 1994 to 2011 to produce substantial overlap with the data set
286 of AERONET AOD measurements. The first year of each simulation was used as model spin-up
287 and thus not used for analysis.
288
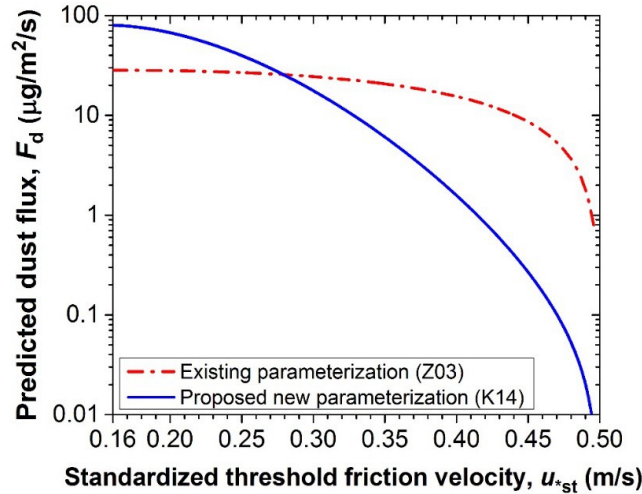
289
290 **Figure 1.** The vertical dust flux (F_d) as a function of the soil's standardized threshold friction
291 velocity (u_{*st}) in CESM for the default Z03 dust flux parameterization (Eq. 6; dash-dotted red
292 line), and for the K14 parameterization (Eq. 7; solid blue line). Results are shown for $u_* = 0.50$

293 m/s and for f_{clay} = 15%, which is a typical value for dust emitting regions (see Fig. S1). The
294 predicted dust fluxes include the global tuning factors that eliminates the bias against AERONET
295 AOD measurements for Simulations I and IV, respectively (see Eq. 1 and Section 2.2.1).
296

297 **2.2. Measurements used to evaluate the representation of dust emission in**
298 **CESM**

299 We evaluate the representation of dust emission in the four dust cycle simulations by comparing
300 their predictions against dust cycle measurements close to source regions. Arguably the best
301 available data to test a model's dust emission scheme are the extensive and accurate (Eck et al.,
302 1999) AOD measurements by the AERONET network (Holben et al., 1998). In addition to these
303 measurements, we also compare the simulation results against a satellite-derived estimate of dust
304 optical depth and dust mass path (DMP) off the West African coast (Evan et al., 2014).
305

306 **2.2.1. AERONET AOD measurements**

307 AERONET sites use sun photometers to measure radiances at a range of wavelengths, which are
308 then inverted to retrieve aerosol properties (Dubovik et al., 2002; Dubovik et al., 2006). For this
309 study, we used the daily-averaged level 2.0 quality-assured AOD (pre and post-field calibrated
310 and manually inspected), obtained from the Version 2 Direct Sun Algorithm.
311 We select 'dusty' AERONET stations by only using stations for which our simulations
312 indicate that over 50% of the annually-averaged AOD is due to dust aerosols (i.e., stations for
313 which at least three of the four simulations find that over 50% of AOD is due to dust for the grid
314 box in which the station is located; see Fig. S2). Furthermore, for each station, we select only
315 days for which the Angstrom exponent α (in the 440-870 nm wavelength range) is smaller than 1
316 (Eck et al., 1999; Dubovik et al., 2002). Since α is a measure of particle size, with smaller values
317 indicating coarser aerosols, values of $\alpha < 1$ indicate that a substantial fraction of AOD is due to
318 dust (Eck et al., 1999; Dubovik et al., 2002), which is a relatively coarse aerosol. Choosing a
319 different plausible cut-off for AE does not qualitatively affect our results. Finally, we select only
320 stations for which at least 6 months of data (i.e., at least 183 days) is available over the
321 simulation period.
322 The above procedure resulted in the selection of 42 'dusty' AERONET stations: 18 in North
323 Africa, 4 in the North Atlantic, 11 in the Middle East, 6 in the rest of Asia, and 3 in Australia
324 (Figs. 3 – 5, S5). Comparisons between simulated and measured AOD at these stations is
325 sensitive to the value of the parameter C_{tune} (see Eq. 1), which scales the size of the global dust
326 cycle. Because of the many uncertainties in parameterizing dust emission on both small scales
327 (Barchyn et al., 2014; Kok et al., 2014) and the much larger global model grid box scale
328 (Cakmur et al., 2004), the value of C_{tune} is poorly constrained (Cakmur et al., 2006; Huneeus et
329 al., 2011). We therefore choose the value of C_{tune} for each of the four simulations such that the
330 bias vanishes. That is, we determine C_{tune} by forcing the average modeled optical depth at
331 AERONET stations to equal the average observed optical depth:

$$\sum_{i}^{N} \tau_{model,i} = \sum_{i}^{N} \tau_{meas,i} \tag{8}$$

,

9

332 where i sums over the $N = 42$ 'dusty' AERONET stations, and τ_{model} is the AOD in the visible
333 wavelength (550 nm) simulated at the AERONET station location, the component of which that
334 is due to dust aerosols scales with C_{tune}. The measured AERONET AOD (τ_{meas}) is obtained at 550
335 nm, the central wavelength in the visible spectrum, by correcting the AOD measured at 675 nm
336 to 550 nm using the measured value of the Angstrom exponent α. That is,

$$\tau_{\text{meas},i} = \tau_{675,i}\left(\frac{\lambda_{675}}{\lambda_{550}}\right)^{\alpha} \qquad (9)$$

337 where τ_{675} is the measured AOD at 675 nm, and λ_{550} and λ_{675} equal 550 and 675 nm, respectively.
338   We use the above procedure to generate three quantitative comparisons between the
339 simulated and the measured AERONET AOD. First, we obtain the measured 'climatological'
340 AOD for each station over the period of the model simulations (1995-2011) by averaging over all
341 days for which AERONET data is available (subject to the quality-control criteria discussed
342 above). For each station, we compare this average measured AOD to the simulated AOD
343 averaged over the same days. Second, we obtain a comparison for the seasonal cycle of AOD by
344 (i) calculating the measured monthly-averaged AOD for months with at least 10 days of data, (ii)
345 calculating the corresponding simulated monthly AOD averaged over the same days, and (iii)
346 averaging all simulated and modeled monthly-averaged AOD values for each of the 12 months in
347 the year, and comparing them. And, third, we obtain a comparison between daily-averaged
348 variations in AOD at each station. In order to prevent mismatches between model time and local
349 time, we restrict the analysis of daily-averaged AOD variations to the 31 stations with longitude
350 between 60W – 60E.
351

352 2.2.2. Satellite-derived estimates of dust mass path (DMP)

353 In addition to assessing the fidelity of the four different dust emission parameterizations through
354 comparisons against AERONET AOD, we use recent satellite-derived estimates of dust optical
355 depth and dust mass path (DMP; g/m^2) off the West African coast around Cape Verde by Evan et
356 al. (2014). This study followed Kaufman et al. (2005) and Evan and Mukhopadhyay (2010) in
357 separating the dust contribution to AOD from the (smaller) contributions of anthropogenic and
358 marine aerosols for the long-term records of the Advanced Very High Resolution Radiometer
359 (AVHRR) and the Moderate Resolution Imaging Spectroradiometer (MODIS) satellites. Evan et
360 al. (2014) subsequently obtained the DMP by using the result of Kaufman et al. (2005) that a unit
361 dust AOD corresponds to 2.7 ± 0.4 g/m^2 of suspended dust. Since DMP simulated at Cape Verde
362 by climate models participating in the Climate Model Intercomparison Phase 5 (CIMP5) is
363 strongly correlated to the simulated total North African emissions (Evan et al., 2014), and since
364 the fraction of AOD contributed by dust in the study area exceeds the 50% threshold for which
365 we consider the area 'dusty'(see Section 2.2.1 and Fig. S2), we use the dust AOD and the DMP
366 off the West African coast as additional tests of the dust emission component of CESM.
367

368   2.3. Other measurements of the dust cycle

369 The measurement comparisons described in the previous section are designed to evaluate
370 possible improvements in CESM's representation of dust emission. This section describes
371 measurement comparisons to test whether such improvements propagate into an improved

372 simulation of dust cycle properties further from source regions. Specifically, we compare the
373 model results against measurements of dust surface concentration (Prospero and Nees, 1986) and
374 deposition (Albani et al., 2014), which are generally taken far from source regions.
375

2.3.1. Surface concentration measurements

377 We compare the simulation results against a data set of dust concentration measurements at the
378 surface. These data are a compilation of measurements taken in the North Atlantic during the
379 Atmosphere-Ocean Chemistry Experiment (AEROCE; Arimoto et al. (1995)) and in the Pacific
380 Ocean during the sea/air exchange program (SEAREX; Prospero et al. (1989)). Since the
381 majority of these stations measure long-range transported dust, the ability of the model to
382 reproduce these measurements depends on the accuracy of model parameterizations of several
383 processes in addition to dust emission, including transport, and wet and dry deposition. We only
384 use stations where CESM predicts at least some dust (> 0.05 µg/m^3 on an annual basis), such that
385 the comparisons between the four simulations are meaningful. This results in a total of 15
386 stations (see Fig. S6).
387   The data sets from AEROCE and SEAREX were obtained by drawing large volumes of air
388 through a filter when the wind was onshore and not very light (i.e., > 1 m/s); this was done to
389 help reduce the effects of anthropogenic aerosols on the measurements (Prospero et al., 1989).
390 The mineral dust fraction of the collected airborne particulates was determined either from their
391 Al content (assumed to be 8%, corresponding to the Al abundance in the Earth's crust), or by
392 burning the sample and assuming the ash residue to represent the mineral dust fraction (Prospero,
393 1999).
394   For each station, we first calculate the average dust concentration for each of the 12 months
395 in the year using the data provided by Joseph Prospero to the AeroCom project (Joseph Prospero
396 and Nicolas Huneeus, personal communication, 2014). We then calculate a 'climatological'
397 average for each site by averaging over the seasonal cycle. We compare these measures to the
398 seasonal cycle and 'climatological' dust concentration predicted by CESM over the period 1995
399 – 2011 (Table 2). We emphasize that, since the data of the AEROCE and SEAREX campaigns
400 were taken for different dates at each site in the period 1981-2000, the 'climatology' derived
401 from these measurements is for a different period than that of the model simulation, introducing
402 systematic errors of unknown size. Similar comparisons in previous studies have suffered from
403 the same problem (e.g., Huneeus et al. (2011); Albani et al. (2014); (Colarco et al., 2014)).
404

2.3.2. Deposition measurements

406 We further compare the simulation results against the data set of dust deposition measurements
407 compiled by Albani et al. (2014), which consists of 110 stations. This compilation was produced
408 by merging pre-existing datasets (Ginoux et al., 2001; Tegen et al., 2002; Lawrence and Neff,
409 2009; Mahowald et al., 2009), and retaining only measurements representative of modern
410 climate (i.e., excluding sites representing a sediment flux integrated over hundreds or thousands
411 of years). Furthermore, the size range of the measured deposition flux was adjusted to be
412 consistent with the dust size range simulated in CESM of $0.1 – 10$ µm (Albani et al., 2014).
413   Since the deposition fluxes represent an integration over long time scales (generally years to
414 decades), we can only compare the global distribution of the deposition fluxes to those simulated
415 by CESM, and cannot compare seasonal or daily variations. Specifically, we compare the

416 measured annual deposition flux at each station against the mean annual deposition flux
417 simulated by CESM with the various dust emission configurations over the period 1995 – 2011
418 (Table 1). As with the concentration comparison, the dates over which the measurements were
419 obtained were by and large not coincident in time with the simulations, introducing systematic
420 errors of unknown size. Furthermore, note that model representation of the dust deposition flux
421 depends on the realistic simulation of a variety of processes. In addition to dust emission and
422 transport, this notably includes wet and dry deposition, which is generally poorly captured by
423 models (Huneeus et al., 2011).
424

425 **2.4. Bootstrapping method to assess statistical significance of model**
426 **improvements**

427 We quantify the model performance for the range of comparisons outlined above by calculating
428 the Pearson correlation coefficient r and the root mean square error (RMSE) (Bevington and
429 Robinson, 2003; Wilks, 2011). An increase in r or a decrease in RMSE thus denotes an
430 improvement in the model's ability to reproduce a given data set. To assess whether such an
431 improvement is statistically significant, we use the *bootstrap method* (Efron, 1982). That is, we
432 randomly select a number of samples from the 'distribution' of the observed data points, equal to
433 the total number of data points. This is done with replacement, such that each data point can be
434 chosen several times, or not at all. For each of the four simulations, we then calculate the value
435 of r and RMSE for the model comparison with this randomly-chosen sample. By repeating this
436 procedure a large number of times, the uncertainty of any arbitrary statistical measure can be
437 estimated (Efron, 1982). In our case, we assess the significance of a model improvement by
438 checking whether the statistical measure (r or RMSE) is improved for $\geq$ 95% of the bootstrap
439 samples, which is equivalent to the p-value of $\leq$ 0.05 generally used to represent statistical
440 significance (e.g., Wilks (2011)). Table S2 lists the p-values of all comparisons between model
441 results reported in Tables 1 and 2.
442

443 # 3. Results

444 This section presents the results of the four simulations. Below, we first present and qualitatively
445 discuss the spatial patterns of the source functions, and the resulting dust emissions and dust
446 AOD. Section 3.2 then reports the quantitative comparison of simulation results against aerosol
447 optical depth measurements in dusty regions, after which Section 3.3 presents comparisons
448 against dust cycle measurements further from source regions (i.e., dust concentration and
449 deposition measurements).
450

451 **3.1. The spatial patterns of source functions, dust emissions, and dust AOD**

452 One of the objectives of the present study is to evaluate the hypothesis that use of the K14
453 scheme reduces the need for a source function in dust cycle simulations. We investigate this
454 hypothesis by comparing the simulated spatial pattern of the dust emission coefficient C_d in K14,
455 which scales the dust flux in Simulation IV, to the Zender et al. (2003b) and Ginoux et al. (2001)
456 source functions (Figs. 2 and S3). As such, we interpret C_d as a physically-based and temporally-
457 variable source function because C_d scales the dust emission flux in K14 in a manner that is
458 similar (but not identical) to that of a source function (compare Eqs. 1 and 7a). We find that the

459   large-scale spatial pattern of C_d, which is highly anti-correlated to the soil moisture content of the
460   top soil layer (Fig. S4), is strikingly similar to that of the Ginoux et al. (2001) source function.
461   That is, although Figs. 2b and 2c can show different patterns within source regions, both show a
462   clear shift of emissions towards the "dust belt" of North Africa and the Middle East. In the case
463   of Fig. 2b (Simulation III), this shift is empirically parameterized based on TOMS satellite
464   observations (Ginoux et al., 2001). In contrast, in Fig. 2c (Simulation IV) this shift arises from
465   the additional physics accounted for in K14 over Z03. Specifically, the shift of emissions to the
466   most erodible regions arises from the greater sensitivity of the dust flux to the soil's threshold
467   friction velocity (Fig. 1), which occurs because K14 accounts for a soil's increased ability to
468   produce dust as it becomes more erodible.
469   The spatial patterns of the source functions and the dust emission coefficient C_d partially
470   determine the dust flux (Figs. 3 and S2a-d), which in turn determines the dust optical depth
471   (Figs. 4 and S2e-h). The simulation results show that application of a source function tends to
472   shift dust emissions (Fig. 3) and dust AOD (Fig. 4) from less erodible regions, such as North
473   America, to more erodible regions, such as North Africa. As hypothesized in our companion
474   paper (Kok et al., 2014), and consistent with the similarity between C_d and the Ginoux et al.
475   (2001) source function (Fig. 2), replacing Z03 with K14 has an effect that is similar to the
476   application of an empirical source function. That is, it shifts emissions and dust AOD to the most
477   erodible regions, producing increases in emissions and AOD over most of North Africa, and
478   decreases over less erodible regions such as North America and Southern Africa (Figs. 3d, 4d).
479   Moreover, K14 shifts dust AOD within North Africa westward, as well as southward towards the
480   $15º – 25º$ N latitude belt. This appears to bring the simulations in better agreement with
481   qualitative satellite observations of North African dust emitting regions (Prospero et al., 2002;
482   Schepanski et al., 2009; Crouvi et al., 2012; Ginoux et al., 2012; Ashpole and Washington,
483   2013). Furthermore, applying K14 substantially increases dust emissions in Patagonia (Figs. 2c,
484   3d, and 4d), which in the default version of CESM needs to be increased by about two orders of
485   magnitude to match available observations (Albani et al., 2014).
486   The simulation results further show that dust emissions depend quite differently on soil
487   properties for the different dust emission schemes. In particular, the soil clay fraction f_{clay} has two
488   competing effects, and the relative strength of these differ between the schemes. On the one
489   hand, f_{clay} scales the threshold moisture content above which additional soil moisture increases
490   the soil's threshold friction velocity (see Eq. 4), and on the other hand f_{clay} scales the dust
491   emission flux (see Eq. 7a). Since the scaling of the dust flux with f_{clay} is exponential in Z03, it
492   overwhelms the effect of f_{clay} on the threshold friction velocity, such that dust fluxes in
493   Simulation I correlate strongly with f_{clay} (compare Figs. 3a and S1). In contrast, in the K14
494   scheme the dust flux scales merely linearly with f_{clay}, such that both effects of the clay fraction on
495   the dust flux are important. Consequently, the effect of f_{clay} on dust emissions in K14 is not
496   straightforward, and the map of Simulation IV's dust emission fluxes (Fig. S2d) does not show
497   an obvious correlation with the map of the clay fraction (Fig. S1). However, because the strong
498   exponential dependence of the dust flux on f_{clay} in Z03 is replaced by a linear dependence in K14,
499   areas with low clay content, such as sand dunes, produce consistently more dust in Simulation IV
500   than in Simulation I (compare Figs. 3d and S1). This brings the results of Simulation IV in better
501   qualitative agreement with the observation by Crouvi et al. (2012) that a large fraction of North
502   African dust plumes originate from sand dunes. Furthermore, since CESM does not use a map of
503   the spatially variable aerodynamic roughness length to more accurately calculate the
504   aerodynamic drag on the bare (erodible) soil, it is likely that improving the model by using such

13

505　a map ([Laurent et al., 2008](); [Menut et al., 2013]()) would produce even higher fluxes in regions
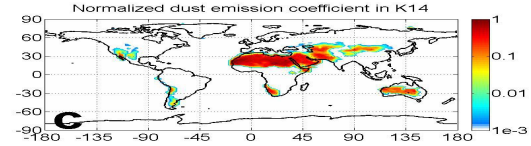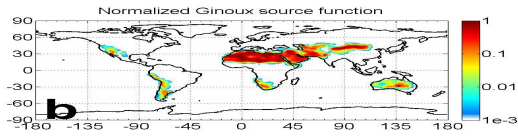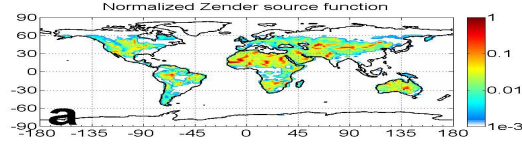506　covered in sand dunes, since these regions tend to have low roughness length.
507

508

509
510　**Figure 2.** Global maps of (**a**) the [Zender et al. (2003b)]() geomorphic source function used in
511　Simulation II, (**b**) the [Ginoux et al. (2001)]() source function used in Simulation III, and (**c**) the
512　K14 dust emission coefficient C_d (see Eq. 7b) averaged over the model run (1995 – 2011). The
513　seasonal cycle of C_d is reported in Fig. S3. Since the [Ginoux et al. (2001)]() source function
514　inherently includes the fraction of the grid cell that consists of bare soil, both the [Zender et al.]()
515　[(2003b)]() source function and the dust emission coefficient C_d were multiplied by the grid cell's
516　bare soil fraction (see Eq. 5). To further facilitate comparison, the source functions and C_d are
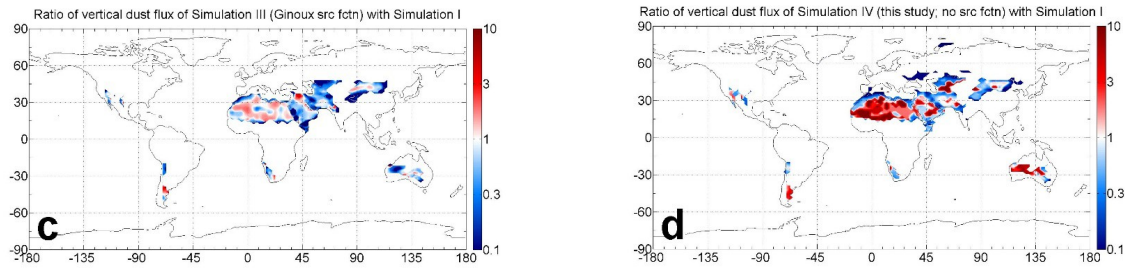517　each normalized by their highest occurrence in any of the grid boxes.
518

519
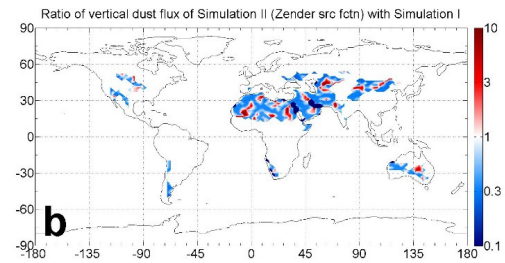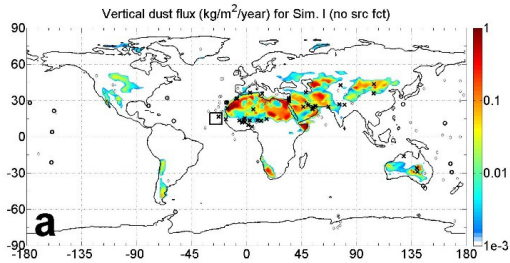
520
Figure 3. Global maps of (**a**) the simulated vertical dust flux for Simulation I and (**b - d**) the ratios of the dust flux in Simulations II – IV to the flux in Simulation I. Red (blue) coloring in panels (**b**) – (**d**) denotes increases (decreases) in dust emission fluxes relative to the 'control' (Simulation I). In panel (**a**), crosses, circles, and diamonds respectively mark the locations of measurements of AERONET AOD, dust surface concentration, and dust deposition flux. The square denotes the area off the West African coast for which the satellite-derived dust AOD and DMP were used.

529
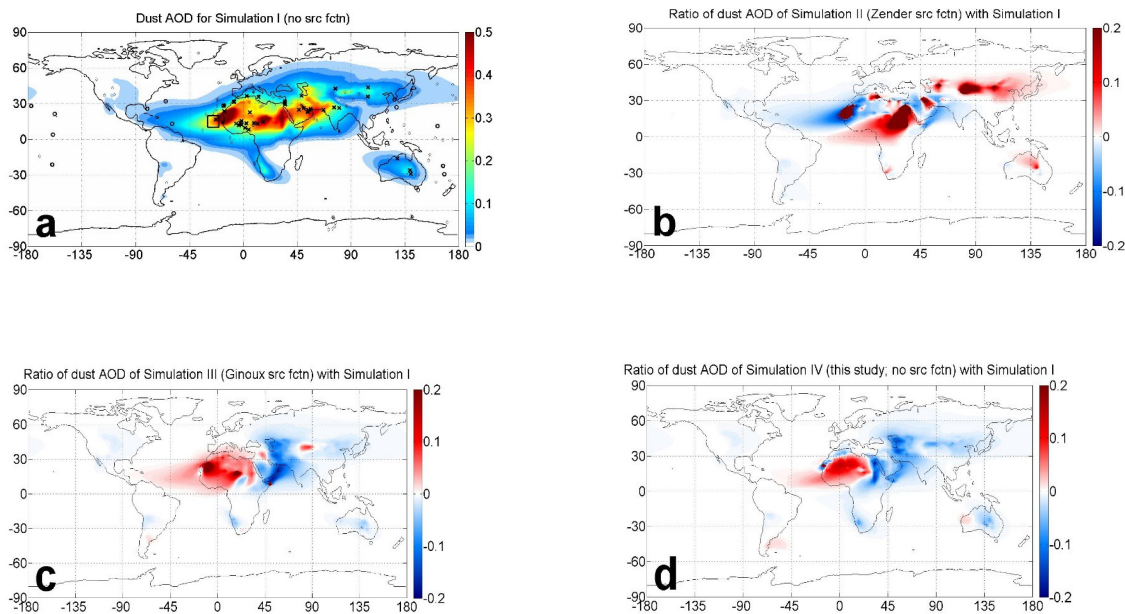
530
Figure 4. Global maps of (**a**) the dust aerosol optical depth (AOD) of Simulation I, and (**b - d**) the difference of dust AOD of Simulations II – IV with that of Simulation I. Red shading denotes increases in dust AOD relative to the 'control' (Simulation I). Black symbols in panel (**a**) are as defined in Fig. 3.

3.2. Measurement comparisons evaluating CESM's representation of dust emission

3.2.1. AOD climatology

15

539 As discussed previously, the data sets of AOD at the 42 'dusty' AERONET stations (see Section
540 2.2.1) are arguably the most reliable currently available data to quantitatively evaluate the dust
541 emission components of large-scale models. We therefore perform an extensive comparison
542 against the AERONET AOD data sets (Table 1 and Figs. 5, S5). As expected, the application of
543 the source functions of both Zender et al. (2003b) and Ginoux et al. (2001) improve model
544 agreement against the average ('climatological') AERONET AOD data (Figs. 5a-c). However, a
545 substantially larger and statistically significant improvement is obtained with Simulation IV,
546 which uses the K14 scheme and does not use a source function (Fig. 5d and Table 1). In
547 particular, Simulation IV produces improved agreement over North Africa, the Middle East, and
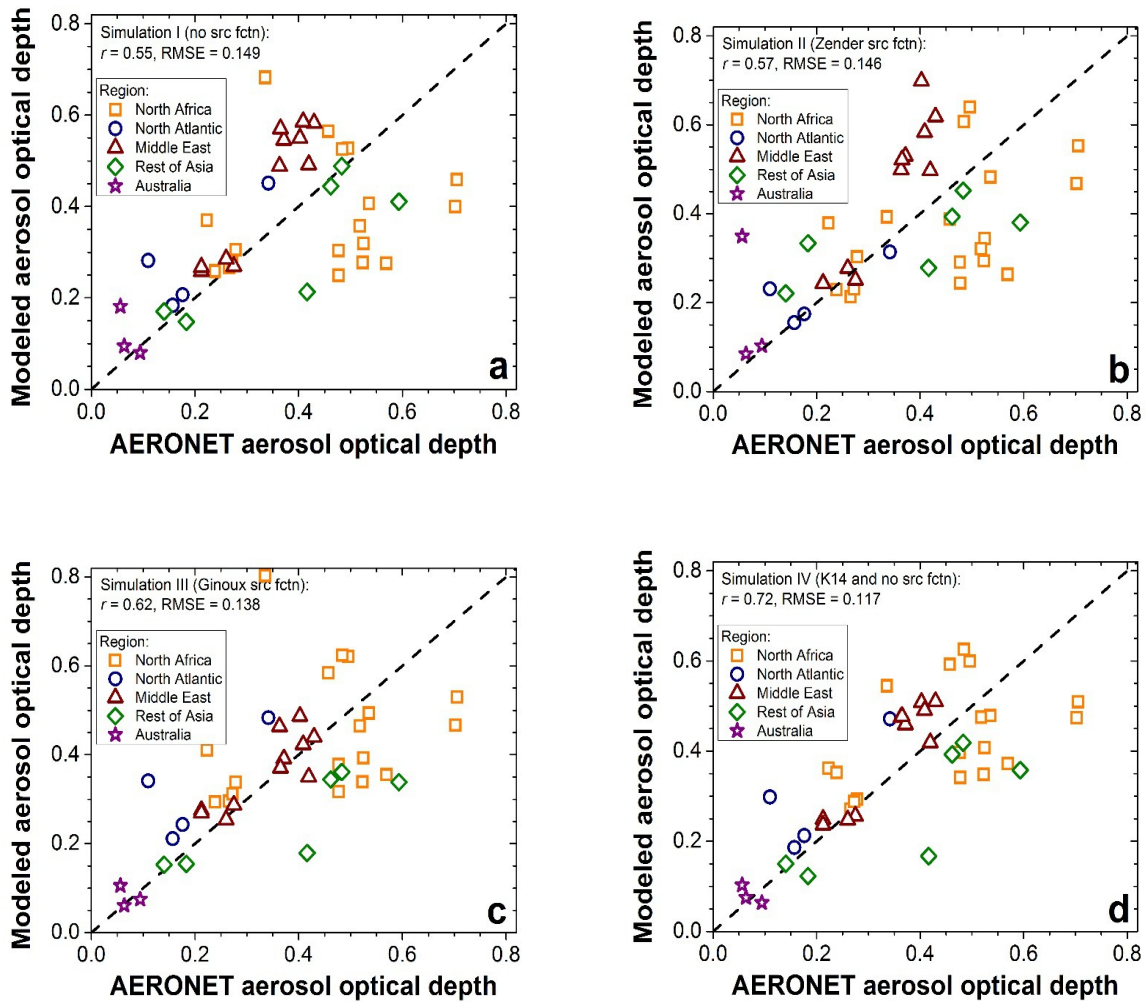548 Australia, and somewhat lesser agreement over Asia.
549
550

551

552
553 **Figure 5.** Comparison of measured and modeled aerosol optical depth (AOD) at 42 dust-
554 dominated AERONET stations. Results are shown for (**a**) Simulation I (no source function), (**b**)
555 Simulation II (Zender et al. (2003b) geomorphic source function), (**c**) Simulation III (Ginoux et
556 al. (2001) source function), and (**d**) Simulation IV (no source function, and dust flux is

557 parameterized following K14 instead of Z03). For each simulation, the root mean square error
558 (RMSE) and correlation coefficient (*r*) are noted.
559

3.2.2. AERONET AOD seasonal cycle and daily variability

561 In addition to improving the representation of AOD climatology, applying K14 also produces a
562 statistically significant improvement of CESM's simulation of the seasonal AOD cycle at the
563 AERONET stations (Fig. S5 and Table 1). Indeed, Simulation IV produces the best seasonal
564 agreement for 25 of the 42 AERONET stations, including 15 of the 18 North African stations
565 (Fig. S5). However, the influence of changes in the emission scheme on seasonal variability
566 appears limited: for a given station, the standard deviation of the four correlations produced by
567 the four different simulations is on average only 0.05, which is only a small fraction of the mean
568 correlation coefficient of ~0.80 (Table 1). This indicates a limited influence of the emission
569 scheme on the seasonal variability of AOD, which is likely primarily controlled by seasonal
570 variations in soil moisture, wind, and vegetative soil cover. Consequently, the statistically
571 significant improvement in Simulation IV's ability to reproduce the seasonal cycle of dust AOD
572 results in only a modest improvement in the correlation coefficient (Table 1).
573   The comparison of model results to the measured daily variability of dust AOD at the
574 different AERONET stations produces results that are qualitatively similar to those for the
575 seasonal cycle. That is, Simulation IV again produces a statistically significant improvement in
576 the model's ability to reproduce the daily AOD variability (Table 1), and produces best
577 agreement at 18 of the 31 available stations, including 13 of the 18 North African stations.
578 However, the emission scheme appears to also have limited influence on the daily AOD
579 variability, which is probably largely controlled by the daily variations in wind speed and in soil
580 moisture, which controls the dust emission threshold (see Section 2.1.1). Indeed, for a given
581 station, the standard deviation of the four correlations produced by the four different simulations
582 is on average only 0.03, which is only a small fraction of the mean correlation coefficient for
583 daily variability of ~0.45 (Table 1). Consequently, the absolute improvement in the correlation
584 coefficient produced by the statistically significant improvement in the model's ability to capture
585 daily variability in the AOD is again modest (Table 1).
586

3.2.3. Dust optical depth and dust mass path off the West African coast

588 Evan et al. (2014) analyzed satellite data to estimate both the dust optical depth and the dust
589 column mass path (DMP) off the West African coast over the region of 10º-20º N, 20º-30º W
590 around Cape Verde. They found that most models that participated in the Coupled Model
591 Intercomparison Project Phase 5 (CMIP5) underestimated the dust optical depth for this region,
592 and that all models substantially underestimated the dust mass path. We find that the dust optical
593 depth in Simulations I, III, and IV are close to the satellite estimates, and that all four simulations
594 produce a DMP that is in better agreement with the satellite estimates than that of the CMIP5
595 models, which includes a previous version of CESM (Fig. 6). As already suggested by Evan et al.
596 (2014), these improvements most likely occur because our newer CESM version uses the size
597 distribution of Kok (2011b), which corrects a bias towards fine dust aerosols in most large-scale
598 models. Consequently, using this size distribution results in a higher dust mass path per unit of
599 dust AOD, which is in better agreement with measurements.
600   Although all four simulations are in better agreement with the Evan et al. (2014) estimates of
601 DMP than the CMIP5 models, Simulations I and II still underestimate the DMP, whereas

17

602   Simulations III and IV are consistent with the lower uncertainty range of the satellite estimates.
603   The likely reason for the improved performance of Simulations III and IV is that these
604   simulations shift emissions towards West Africa (see Figs. 2 – 4), resulting in a higher, and thus
605   more realistic, value of DMP off the West African coast.
606   Note that the simulated values of DMP and the dust AOD in Fig. 6 both depend on the tuning
607   constant C_{tune} scaling the dust emissions (see Eqs. 1 and 8). It's thus possible to obtain better
608   agreement with these measures by choosing a different method to set C_{tune}, although doing so
609   would degrade the model's comparison against AERONET AOD (Figs. 5, S5). Also note that the
610   dust optical depth and dust emissions are sensitive to dust radiative effects and dust optical
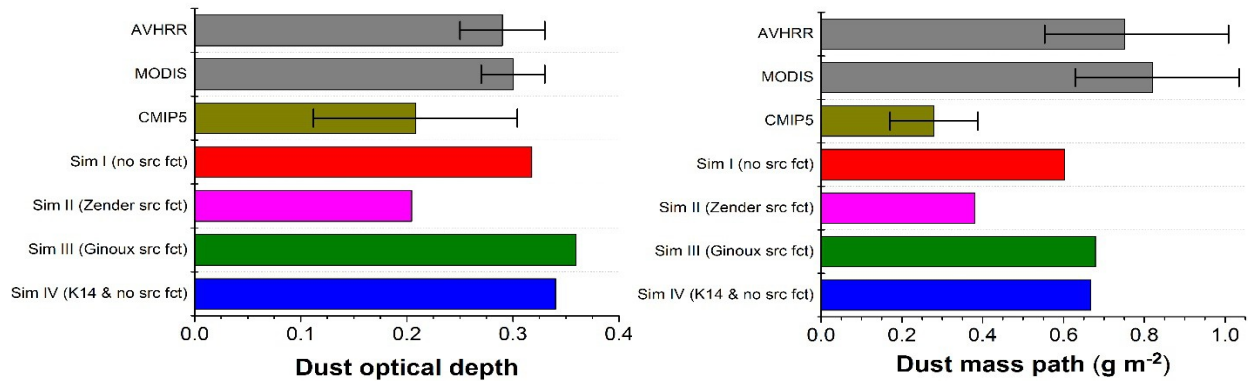611   properties (Perlwitz et al., 2001; Albani et al., 2014).
612

613
614   **Figure 6.** Dust optical depth (left) and dust mass path (right) averaged over the region 10˚-20˚ N
615   and 20˚-30˚ W. Satellite-derived estimates for AVHRR (1982-2005) and MODIS (2001-2012), as
616   well as the ensemble average of CMIP5 models (1982-2005), are from Evan et al. (2014). Error
617   bars denote the uncertainty on the satellite estimates, and the standard deviation of the available
618   CMIP5 model results (23 models for the dust optical depth, and 11 models for the dust mass
619   path; see Evan et al. (2014)). The dust optical depth and dust mass paths calculated from the four
620   CESM simulations were averaged over the period 2001 – 2011 to be most comparable to the
621   MODIS results.
622

623   **3.3. Comparisons against other measurements of the dust cycle**

624   The previous section evaluated possible improvements in CESM's representation of dust
625   emission through comparisons against measurements of aerosol optical depth close to source
626   regions. In this section, we evaluate whether these improvements propagate into the simulation
627   of other dust cycle properties further from source regions. Specifically, we compare the
628   simulation results against measurements of dust surface concentration and deposition, which are
629   generally taken further from source regions (Table 2). We find that Simulation IV, which uses the
630   K14 scheme, produces a statistically insignificant improvement against both the surface dust
631   concentration climatology and seasonal cycle (Figs. 7 and S6). We also find that Simulation IV
632   produces agreement against dust deposition flux measurements that is slightly less than that of
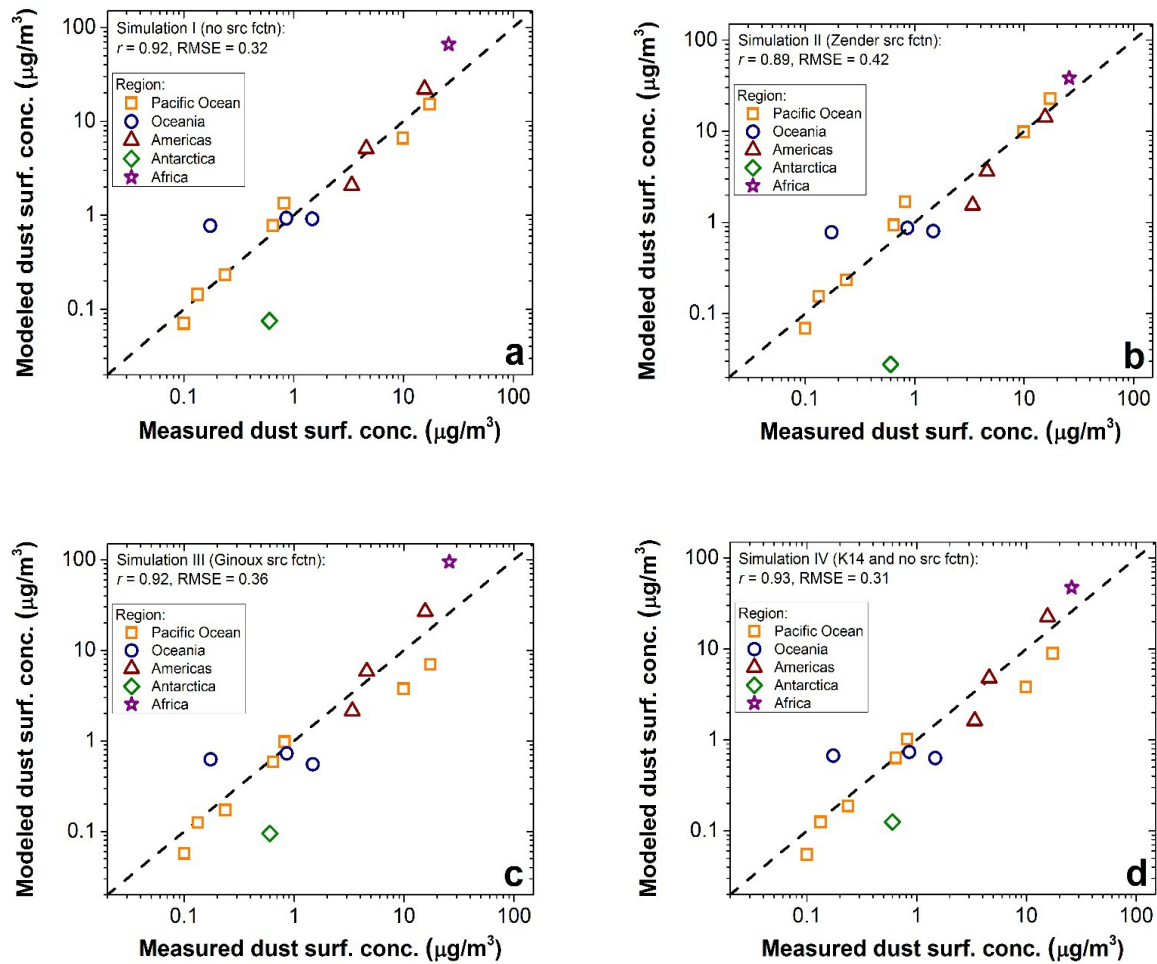633   the other simulations (Fig. 8).
634

18

635

636
637
Figure 7: Comparison of the annually-averaged modeled dust surface concentration with that
measured at 15 stations (see Section 2.3.1). Results are shown for (**a**) Simulation I (no source
function), (**b**) Simulation II (Zender et al. (2003b) source function), (**c**) Simulation III (Ginoux et
al. (2001) source function), and (**d**) Simulation IV (no source function, and dust flux is
parameterized following K14 instead of Z03). For each panel, the root mean square error
(RMSE) and correlation coefficient (*r*) in log10-space are noted.

644
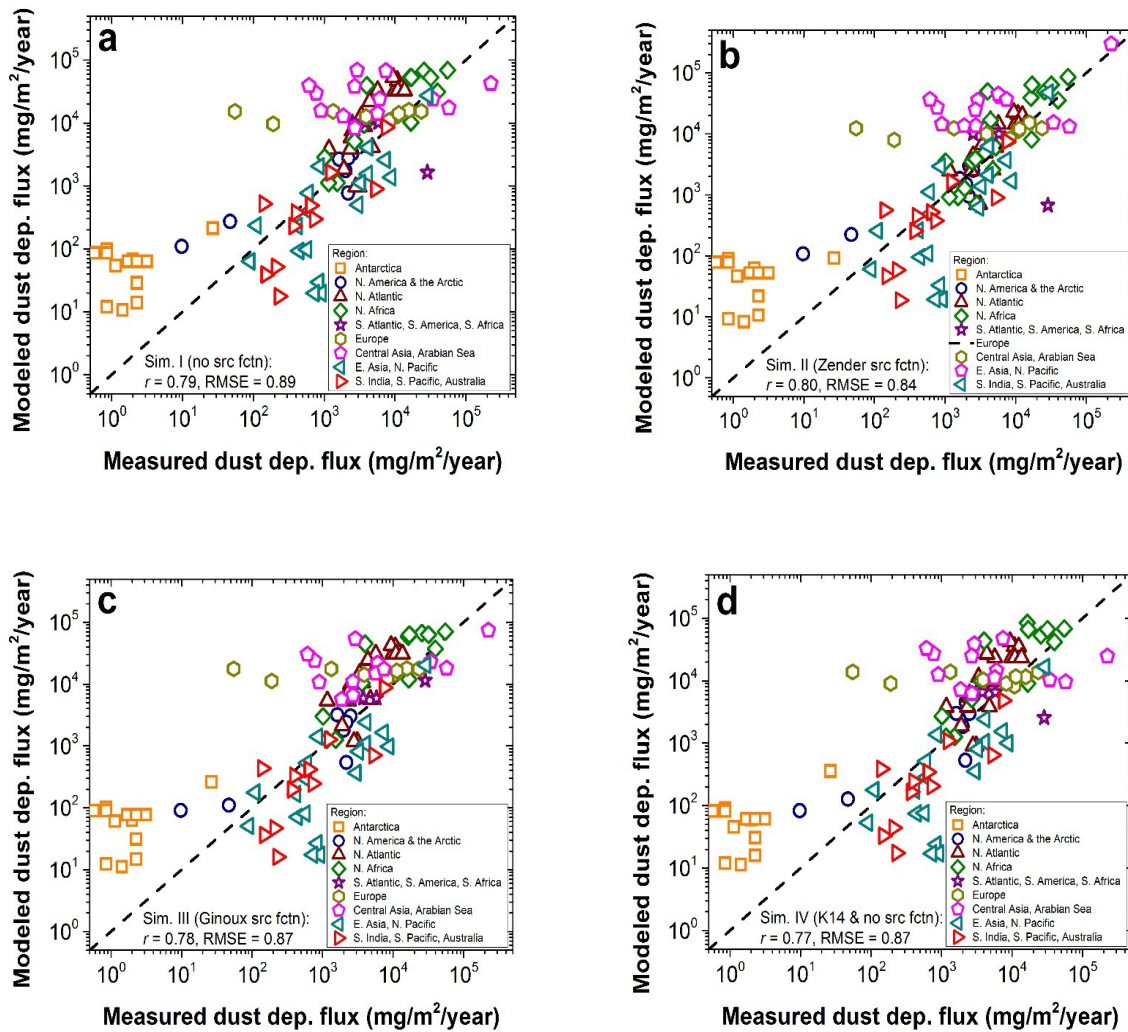
Figure 8: Comparison of the modeled dust deposition flux with that measured at 110 stations (see Section 2.3.2). Results are shown for (**a**) Simulation I (no source function), (**b**) Simulation II (Zender et al. (2003b) source function), (**c**) Simulation III (Ginoux et al. (2001) source function), and (**d**) Simulation IV (no source function, and dust flux is parameterized following K14 instead of Z03). For each panel, the root mean square error (RMSE) and correlation coefficient (*r*) in log10-space are noted.

Table 2. Statistics of the comparison of the four CESM simulations against data sets taken further from source regions, namely dust surface concentration measurements and dust deposition fluxes. Simulations and measurements are compared with respect to their climatology for both data sets and their seasonal cycle for the surface concentration. Statistically significant improvements (see Section 2.4) of Simulations II-IV relative to the 'control' Simulation I are indicated with bold font. Additionally, simulation results that are statistically significantly improved over the results of each of the other three simulations are both bold and underlined.

Simulation	Dust flux parameter-	Dust source	Surf. conc. climatology,	Surf. conc. climatology,	Surf. conc. seasonal	Dep. flux climatology, *r*	Dep. flux climatology,

20

	ization	function	r	RMSE	cycle, r		RMSE
I	Zender et al. (2003a)	None	0.92	0.32	0.62	0.79	0.88
II	Zender et al. (2003a)	Zender et al. (2003b)	0.88	0.42	0.61	**0.80**	**0.84**
III	Zender et al. (2003a)	Ginoux et al. (2001)	0.92	0.36	0.63	0.78	0.87
IV	Kok et al. (2014)	None	0.93	0.31	0.63	0.77	0.87

4. Discussion

The simulations reported in the previous section were designed to (i) evaluate the performance of the K14 dust emission scheme in CESM, and (ii) test the hypothesis in Kok et al. (2014) that the K14 scheme reduces the need to use a source function in dust cycle simulations. The next two sections discuss these two objectives, after which we discuss the implications of our results for the dust cycle's sensitivity to climate changes.

4.1. Evaluation of the K14 dust emission scheme in CESM

Relative to the 'control' (Sim. I), the simulation using K14 (Sim. IV) shows statistically significant improvements against measurements most characteristic of dust emission, namely (i) AERONET AOD climatology (Fig. 5), (ii) variations in AERONET AOD on daily and seasonal timescales (Table 1 and Fig. S5), and (iii) satellite-derived estimates of dust optical depth and dust mass path off the West African coast (Fig. 6). The representation of dust emission in Simulation IV is also statistically significantly improved over the simulations using either the Zender et al. (2003b) or the Ginoux et al. (2001) source function.
     We find that the improvement in CESM's dust emission module by the K14 scheme does not propagate into a statistically significant improvement of the model's ability to reproduce surface measurements of dust concentration (Figs. 7 and S6), or of dust deposition (Fig. 8). Since most stations in these data sets are far from source regions, this indicates that the improvement in CESM's dust emission scheme does not produce comparable improvements in simulated dust cycle properties further from source regions. This could be caused by model errors in other processes, particularly in dust transport and deposition. This is especially likely to explain the lack of improvement in the simulated dust deposition fluxes, which is known to be subject to large model errors (Huneeus et al., 2011). In addition, it is possible that tuning of parameters describing processes such as transport and deposition in previous model versions (e.g., Albani et al. (2014)) degrades the model performance with the new K14 parameterization.

4.2. Does the K14 scheme reduce the need to use a dust source function?

The main reason for the improved representation of dust emissions with K14 is likely that this scheme accounts for a soil's increased ability to produce dust as its erodibility increases (Kok et al., 2014). This results in an increased sensitivity of the dust flux to a soil's standardized dust emission threshold (Fig. 1), which quantifies a soil's susceptibility to wind erosion. Since the dust emission threshold in CESM is parameterized mainly in terms of soil moisture, the dust emission coefficient in the K14 scheme (Fig. 2c) is strongly anti-correlated with soil moisture

697 (Fig. S4). Consequently, relative to the 'control' simulation with the Z03 scheme, the simulation
698 with K14 produces a shift of emissions and dust AOD to hyper-arid - and thus typically highly
699 erodible - regions such as North Africa (Figs. 2c, 3d, 4d). This effect is remarkably similar to that
700 of applying the Ginoux et al. (2001) source function (Figs. 2b, 3c, 4c), which was developed to
701 shift emissions to regions with high dust loadings observed by the TOMS satellite (Prospero et
702 al., 2002). This similarity between the effects of the K14 scheme and the Ginoux et al. (2001)
703 source function suggests that the K14 scheme replaces some of the empiricism introduced by this
704 source function with an improved description of the physics of dust emission.
705   The K14 scheme thus reduces, or even eliminates, the need to use a source function in
706 CESM. Although further work is needed to investigate whether the K14 scheme produces similar
707 improvements in other large-scale models, the additional dust emission physics accounted for in
708 K14 could aid in moving dust modules beyond the widespread use of empirical source functions.
709 Such a transition towards a more physically-explicit treatment of dust emission is necessary for
710 better understanding past and forecasting future changes in the global dust cycle: although
711 empirical descriptions of dust emission can work well for the current climate, such descriptions
712 are unlikely to accurately capture the effect of climate-driven changes in soil erodibility and
713 other relevant factors.
714   Note that parallel efforts to improve the fidelity of dust modules might also help to reduce the
715 reliance on empirical source functions in dust cycle simulations. Indeed, since many source
716 functions were formulated for models that did not account for the spatial variability of the
717 aerodynamic roughness length (Ginoux et al., 2001; Tegen et al., 2002; Zender et al., 2003b), the
718 use of drag partition schemes employing high-resolution maps of roughness length (Laurent et
719 al., 2008; Chappell et al., 2010; Menut et al., 2013) might be particularly effective. In addition, a
720 more accurate description of the land surface through higher resolution and more detailed soil
721 data sets could further reduce the reliance on empirical parameterizations in dust modules.
722

723 **4.3.Implications for the dust cycle's sensitivity to climate changes**

724 An important result from Kok et al. (2014) is that current parameterizations in climate models
725 likely underestimate the dust flux's sensitivity to the soil's threshold friction velocity, which is
726 further supported by the results presented here (Figs. 1 - 4). This underestimation might have
727 important implications for evaluating the global dust cycle's response to climate changes. In
728 particular, since soil erodibility is affected by climate, which partially determines the soil
729 moisture content, aggregation state, and crusting of the soil (Zobeck, 1991; Kok et al., 2012), our
730 results here and in Kok et al. (2014) suggest that many climate models underestimate the dust
731 cycle's climate sensitivity.
732   This result could help explain a series of observations. For instance, climate models have
733 difficulty reproducing the increase in North African dust emissions during the Sahel drought in
734 the 1980s (Mahowald et al., 2002; Evan et al., 2014; Ridley et al., 2014), which is likely partially
735 due to the underestimation of the dust flux's sensitivity to drought conditions (Fig. 1).
736 Furthermore, an increased sensitivity of dust emissions to climate changes could help explain the
737 large differences in the global dust cycle between different climates, such as the much larger dust
738 deposition fluxes measured for the Last Glacial Maximum (Rea, 1994; Harrison et al., 2001),
739 which climate models also have difficulty reproducing without positing large changes in source
740 areas (Werner et al., 2002; Mahowald et al., 2006b).
741

5. Summary and Conclusions

We used CESM simulations to both evaluate the performance of the K14 dust emission scheme developed in the companion paper (Kok et al., 2014), and to test the hypothesis that the K14 scheme reduces the need to use an empirical source function in dust cycle simulations.

We find that implementing the K14 scheme has an effect that is strikingly similar to that of implementing the Ginoux et al. (2001) source function. That is, it shifts emissions and dust AOD towards the most erodible regions, especially North Africa (Figs. 2- 4). Indeed, the spatial pattern of the dust emission coefficient C_d, which scales the dust flux in K14 using only the dust emission threshold and can thus be interpreted as a physically-based and dynamic source function, is remarkably similar to that of the Ginoux et al. (2001) source function (Fig. 2). We further find that the K14 scheme improves CESM's representation of dust emission, as evidenced by statistically significant improvements of the model's ability to reproduce AERONET AOD measurements in dusty regions (Table 1, Figs. 5, S5) and satellite observations of dust optical depth and dust mass path off the West African coast (Fig. 6). These improvement substantially exceed those produced by implementing either the Zender et al. (2003b) or the Ginoux et al. (2001) source functions.

These results suggest that the K14 scheme replaces some of the empiricism introduced by the use of a source function with an improved description of the physics of dust emission. As such, the K14 scheme reduces, or even eliminates, the need to use a source function in dust cycle simulations in CESM. Further work is required to investigate whether the K14 scheme can similarly improve other large-scale models.

Our results further suggest that many large-scale models have used source functions to empirically account for a part of the sensitivity of the dust flux to the soil threshold friction velocity (Figs. 1 – 4). Because climate changes affect this dust emission threshold, for instance by affecting the soil moisture content and soil aggregation (Zobeck, 1991; Fecan et al., 1999; Shao, 2008; Kok et al., 2012), many models might underestimate the dust cycle's sensitivity to climate changes. Since the K14 scheme accounts for this missing component of the dust flux' sensitivity to the soil threshold friction velocity, namely the effect that a more erodible soil will produce more dust per saltator impact (Kok et al., 2014), we expect that it can improve the accuracy of dust cycle simulations for past and future climates.

Accounting for the dust flux's increased sensitivity to the soil state will thus affect simulations of the global dust cycle's response to future climate changes. In particular, since arid regions are generally predicted to become drier in most climate models (Solomon et al., 2007), accounting for the dust flux' increased sensitivity to the soil threshold friction velocity would likely produce an increase in the future global dust emission rate, and thus in the global dust radiative forcing, relative to simulations that do not account for this. Since the dust cycle is sensitive to a variety of processes, including CO_2 fertilization (Mahowald et al., 2006b), land use change (Ginoux et al., 2012), and changes in sediment availability (Harrison et al., 2001), a substantial body of further work is required to assess the dust cycle's response to future climate changes.

23

References

Albani, S., Mahowald, N. M., Perry, A. T., Scanza, R. A., Zender, C. S., Heavens, N. G., Maggi, V., Kok, J. F., and Otto-Bliesner, B. L.: Improved dust representation in the Community Atmosphere Model, J. Adv. Model. Earth Syst., doi: 10.1002/2013MS000279, 2014. 2014.

Andronache, C.: Estimated variability of below-cloud aerosol removal by rainfall for observed aerosol size distributions, Atmospheric Chemistry and Physics, 3, 131-143, 2003.

Arimoto, R., Duce, R. A., Ray, B. J., Ellis, W. G., Cullen, J. D., and Merrill, J. T.: Trace-elements in the atmosphere over the north-atlantic, Journal of Geophysical Research-Atmospheres, 100, 1199-1213, 1995.

Ashpole, I. and Washington, R.: A new high-resolution central and western Saharan summertime dust source map from automated satellite dust plume tracking, Journal of Geophysical Research-Atmospheres, 118, 6981-6995, 2013.

Balkanski, Y. J., Jacob, D. J., Gardner, G. M., Graustein, W. C., and Turekian, K. K.: Transport and residence times of tropospheric aerosols inferred from a global 3-dimensional simulation of pb-210, Journal of Geophysical Research-Atmospheres, 98, 20573-20586, 1993.

Barchyn, T. E., Martin, R., Kok, J., and Hugenholtz, C. H.: Fundamental mismatches between measurements and models in aeolian sediment transport prediction: The role of small-scale variability, Aeolian Research, in press, 2014.

Bevington, P. R. and Robinson, D. K.: Data reduction and error analysis, McGraw-Hill, New York, 2003.

Cakmur, R. V., Miller, R. L., Perlwitz, J., Geogdzhayev, I. V., Ginoux, P., Koch, D., Kohfeld, K. E., Tegen, I., and Zender, C. S.: Constraining the magnitude of the global dust cycle by minimizing the difference between a model and observations, Journal of Geophysical Research-Atmospheres, 111, D06207, 2006.

Cakmur, R. V., Miller, R. L., and Torres, O.: Incorporating the effect of small-scale circulations upon dust emission in an atmospheric general circulation model, Journal of Geophysical Research-Atmospheres, 109, 2004.

Chappell, A., Van Pelt, S., Zobeck, T., and Dong, Z. B.: Estimating aerodynamic resistance of rough surfaces using angular reflectance, Remote Sensing of Environment, 114, 1462-1470, 2010.

Claquin, T., Schulz, M., and Balkanski, Y. J.: Modeling the mineralogy of atmospheric dust sources, Journal of Geophysical Research-Atmospheres, 104, 22243-22256, 1999.

Colarco, P. R., Nowottnick, E. P., Randles, C. A., Yi, B. Q., Yang, P., Kim, K. M., Smith, J. A., and Bardeen, C. G.: Impact of radiatively interactive dust aerosols in the NASA GEOS-5 climate model: Sensitivity to dust particle shape and refractive index, Journal of Geophysical Research-Atmospheres, 119, 753-786, 2014.

Crouvi, O., Schepanski, K., Amit, R., Gillespie, A. R., and Enzel, Y.: Multiple dust sources in the Sahara Desert: The importance of sand dunes, Geophysical Research Letters, 39, 2012.

Dee, D. P., Uppala, S. M., Simmons, A. J., Berrisford, P., Poli, P., Kobayashi, S., Andrae, U., Balmaseda, M. A., Balsamo, G., Bauer, P., Bechtold, P., Beljaars, A. C. M., van de Berg, L., Bidlot, J., Bormann, N., Delsol, C., Dragani, R., Fuentes, M., Geer, A. J., Haimberger, L., Healy, S. B., Hersbach, H., Holm, E. V., Isaksen, L., Kallberg, P., Kohler, M., Matricardi, M., McNally, A. P., Monge-Sanz, B. M., Morcrette, J. J., Park, B. K., Peubey, C., de Rosnay, P., Tavolato, C., Thepaut, J. N., and Vitart, F.: The ERA-Interim reanalysis: configuration and performance of the data assimilation system, Quarterly Journal of the Royal Meteorological Society, 137, 553-597, 2011.

25

840   Dubovik, O., Holben, B., Eck, T. F., Smirnov, A., Kaufman, Y. J., King, M. D., Tanre, D., and
841   Slutsker, I.: Variability of absorption and optical properties of key aerosol types observed in
842   worldwide locations, J. Atmos. Sci., 59, 590-608, 2002.
843   Dubovik, O., Sinyuk, A., Lapyonok, T., Holben, B. N., Mishchenko, M., Yang, P., Eck, T. F.,
844   Volten, H., Munoz, O., Veihelmann, B., van der Zande, W. J., Leon, J. F., Sorokin, M., and
845   Slutsker, I.: Application of spheroid models to account for aerosol particle nonsphericity in
846   remote sensing of desert dust, Journal of Geophysical Research-Atmospheres, 111, D11208,
847   2006.
848   Eck, T. F., Holben, B. N., Reid, J. S., Dubovik, O., Smirnov, A., O'Neill, N. T., Slutsker, I., and
849   Kinne, S.: Wavelength dependence of the optical depth of biomass burning, urban, and desert
850   dust aerosols, Journal of Geophysical Research-Atmospheres, 104, 31333-31349, 1999.
851   Efron, B.: The jackknife, the bootstrap, and other resampling plans, Capital City Press,
852   Montpelier, Vermont, 1982.
853   Evan, A. T., Flamant, C., Fiedler, S., and Doherty, O.: An analysis of aeolian dust in climate
854   models, Geophysical Research Letters, doi: 10.1002/2014GL060545, 2014. 2014.
855   Evan, A. T. and Mukhopadhyay, S.: African Dust over the Northern Tropical Atlantic: 1955-
856   2008, Journal of Applied Meteorology and Climatology, 49, 2213-2229, 2010.
857   FAO: Harmonized World Soil Database (version 1.2), FAO, Rome, Italy and IIASA, Laxenburg,
858   Austria, 2012.
859   Fecan, F., Marticorena, B., and Bergametti, G.: Parametrization of the increase of the aeolian
860   erosion threshold wind friction velocity due to soil moisture for arid and semi-arid areas, Ann
861   Geophys-Atm Hydr, 17, 149-157, 1999.
862   Forster, P., Ramaswamy, V., Artaxo, P., Berntsen, T., Betts, R., Fahey, D. W., Haywood, J., Lean,
863   J., Lowe, D. C., Myhre, G., Nganga, J., Prinn, R., Raga, G., Schulz, M., and Dorland, R. V.:
864   Changes in Atmospheric Constituents and in Radiative Forcing. In: Climate Change 2007: The
865   Physical Science Basis., Solomon, S., D. Qin, M. Manning, Z. Chen, M. Marquis, K.B. Averyt,
866   M.Tignor and H.L. Miller (Ed.), Cambridge University Press, Cambridge, United Kingdom and
867   New York, NY, USA, 2007.
868   Gillette, D. A.: Environmental factors affecting dust emission by wind erosion. In: Saharan dust,
869   Morales, C. (Ed.), Wiley, New York, 1979.
870   Gillette, D. A. and Passi, R.: Modeling dust emission caused by wind erosion, Journal of
871   Geophysical Research-Atmospheres, 93, 14233-14242, 1988.
872   Ginoux, P., Chin, M., Tegen, I., Prospero, J. M., Holben, B., Dubovik, O., and Lin, S. J.: Sources
873   and distributions of dust aerosols simulated with the GOCART model, J. Geophys. Res., 106,
874   20255-20273, 2001.
875   Ginoux, P., Prospero, J. M., Gill, T. E., Hsu, N. C., and Zhao, M.: Global-scale attribution of
876   anthropogenic and natural dust sources and their emission rates based on MODIS Deep Blue
877   aerosol products, Reviews of Geophysics, 50, Rg3005, 2012.
878   Grini, A., Myhre, G., Zender, C. S., and Isaksen, I. S. A.: Model simulations of dust sources and
879   transport in the global atmosphere: Effects of soil erodibility and wind speed variability, Journal
880   of Geophysical Research-Atmospheres, 110, 2005.
881   Harrison, S. P., Kohfeld, K. E., Roelandt, C., and Claquin, T.: The role of dust in climate changes
882   today, at the last glacial maximum and in the future, Earth-Sci. Rev., 54, 43-80, 2001.
883   Holben, B. N., Eck, T. F., Slutsker, I., Tanre, D., Buis, J. P., Setzer, A., Vermote, E., Reagan, J. A.,
884   Kaufman, Y. J., Nakajima, T., Lavenu, F., Jankowiak, I., and Smirnov, A.: AERONET - A

885 federated instrument network and data archive for aerosol characterization, Remote Sensing of
886 Environment, 66, 1-16, 1998.
887 Huneeus, N., Schulz, M., Balkanski, Y., Griesfeller, J., Prospero, J., Kinne, S., Bauer, S.,
888 Boucher, O., Chin, M., Dentener, F., Diehl, T., Easter, R., Fillmore, D., Ghan, S., Ginoux, P.,
889 Grini, A., Horowitz, L., Koch, D., Krol, M. C., Landing, W., Liu, X., Mahowald, N., Miller, R.,
890 Morcrette, J. J., Myhre, G., Penner, J., Perlwitz, J., Stier, P., Takemura, T., and Zender, C. S.:
891 Global dust model intercomparison in AeroCom phase I, Atmospheric Chemistry and Physics,
892 11, 7781-7816, 2011.
893 Hurrell, J. W., Holland, M. M., Gent, P. R., Ghan, S., Kay, J. E., Kushner, P. J., Lamarque, J. F.,
894 Large, W. G., Lawrence, D., Lindsay, K., Lipscomb, W. H., Long, M. C., Mahowald, N., Marsh,
895 D. R., Neale, R. B., Rasch, P., Vavrus, S., Vertenstein, M., Bader, D., Collins, W. D., Hack, J. J.,
896 Kiehl, J., and Marshall, S.: The Community Earth System Model A Framework for Collaborative
897 Research, Bulletin of the American Meteorological Society, 94, 1339-1360, 2013.
898 Iversen, J. D. and White, B. R.: Saltation threshold on earth, mars and venus, Sedimentology, 29,
899 111-119, 1982.
900 Jansen, E., Overpeck, J., Briffa, K. R., Duplessy, J.-C., Joos, F., Masson-Delmotte, V., Olago, D.,
901 Otto-Bliesner, B., Peltier, W. R., Rahmstorf, S., Ramesh, R., Raynaud, D., Rind, D., Solomina,
902 O., Villalba, R., and Zhang, D.: Palaeoclimate. In: Climate Change 2007: The Physical Science
903 Basis. Contribution of Working Group I to the Fourth Assessment Report of the
904 Intergovernmental Panel on Climate Change, Solomon, S., Qin, D., Manning, M., Chen, Z.,
905 Marquis, M., Averyt, K. B., Tignor, M., and Miller, H. L. (Eds.), Cambridge University Press,
906 Cambridge, United Kingdom and New York, NY, USA, 2007.
907 Kaufman, Y. J., Koren, I., Remer, L. A., Tanre, D., Ginoux, P., and Fan, S.: Dust transport and
908 deposition observed from the Terra-Moderate Resolution Imaging Spectroradiometer (MODIS)
909 spacecraft over the Atlantic ocean, Journal of Geophysical Research-Atmospheres, 110, 2005.
910 Kok, J. F.: Does the size distribution of mineral dust aerosols depend on the wind speed at
911 emission?, Atmospheric Chemistry and Physics, 11, 10149-10156, 2011a.
912 Kok, J. F.: A scaling theory for the size distribution of emitted dust aerosols suggests climate
913 models underestimate the size of the global dust cycle, Proc. Natl. Acad. Sci. U. S. A., 108,
914 1016-1021, 2011b.
915 Kok, J. F., Mahowald, N. M., Fratini, G., Gillies, J. A., Ishizuka, M., Leys, J. F., Mikami, M.,
916 Park, M.-S., Park, S.-U., Van Pelt, R. S., and Zobeck, T. M.: An improved dust emission model.
917 Part 1: Model description and comparison against measurements, Atmospheric Chemistry and
918 Physics, this issue, 2014.
919 Kok, J. F., Parteli, E. J. R., Michaels, T. I., and Karam, D. B.: The physics of wind-blown sand
920 and dust, Reports on Progress in Physics, 75, 106901, 2012.
921 Koven, C. D. and Fung, I.: Identifying global dust source areas using high-resolution land
922 surface form, Journal of Geophysical Research-Atmospheres, 113, 2008.
923 Laurent, B., Marticorena, B., Bergametti, G., Leon, J. F., and Mahowald, N. M.: Modeling
924 mineral dust emissions from the Sahara desert using new surface properties and soil database,
925 Journal of Geophysical Research-Atmospheres, 113, 2008.
926 Lawrence, C. R. and Neff, J. C.: The contemporary physical and chemical flux of aeolian dust: A
927 synthesis of direct measurements of dust deposition, Chemical Geology, 267, 46-63, 2009.
928 Lawrence, D. M., Oleson, K. W., Flanner, M. G., Thornton, P. E., Swenson, S. C., Lawrence, P.
929 J., Zeng, X. B., Yang, Z. L., Levis, S., Sakaguchi, K., Bonan, G. B., and Slater, A. G.:

930 Parameterization Improvements and Functional and Structural Advances in Version 4 of the
931 Community Land Model, J. Adv. Model. Earth Syst., 3, 27, 2011.
932 Liu, X., Easter, R. C., Ghan, S. J., Zaveri, R., Rasch, P., Shi, X., Lamarque, J. F., Gettelman, A.,
933 Morrison, H., Vitt, F., Conley, A., Park, S., Neale, R., Hannay, C., Ekman, A. M. L., Hess, P.,
934 Mahowald, N., Collins, W., Iacono, M. J., Bretherton, C. S., Flanner, M. G., and Mitchell, D.:
935 Toward a minimal representation of aerosols in climate models: description and evaluation in the
936 Community Atmosphere Model CAM5, Geoscientific Model Development, 5, 709-739, 2012.
937 Ma, P.-L., Rasch, P. J., Wang, H., Zhang, K., Easter, R. C., Tilmes, S., Fast, J. D., Liu, X., Yoon,
938 J.-H., and Lamarque, J.-F.: The role of circulation features on black carbon transport into the
939 Arctic in the Community Atmosphere Model version 5 (CAM5), Journal of geophysical
940 research: Atmospheres, 118, 4657-4669, 2013.
941 Mahowald, N. M., Albani, S., Kok, J. F., Engelstaedter, S., Scanza, R., Ward, D. S., and Flanner,
942 M. G.: The size distribution of desert dust aerosols and its impact on the Earth system, Aeolian
943 Research, doi: 10.1016/j.aeolia.2013.09.002, 2014. 2014.
944 Mahowald, N. M. and Dufresne, J. L.: Sensitivity of TOMS aerosol index to boundary layer
945 height: Implications for detection of mineral aerosol sources, Geophysical Research Letters, 31,
946 2004.
947 Mahowald, N. M., Engelstaedter, S., Luo, C., Sealy, A., Artaxo, P., Benitez-Nelson, C., Bonnet,
948 S., Chen, Y., Chuang, P. Y., Cohen, D. D., Dulac, F., Herut, B., Johansen, A. M., Kubilay, N.,
949 Losno, R., Maenhaut, W., Paytan, A., Prospero, J. A., Shank, L. M., and Siefert, R. L.:
950 Atmospheric Iron Deposition: Global Distribution, Variability, and Human Perturbations, Annual
951 Review of Marine Science, 1, 245-278, 2009.
952 Mahowald, N. M., Kloster, S., Engelstaedter, S., Moore, J. K., Mukhopadhyay, S., McConnell, J.
953 R., Albani, S., Doney, S. C., Bhattacharya, A., Curran, M. A. J., Flanner, M. G., Hoffman, F. M.,
954 Lawrence, D. M., Lindsay, K., Mayewski, P. A., Neff, J., Rothenberg, D., Thomas, E., Thornton,
955 P. E., and Zender, C. S.: Observed 20th century desert dust variability: impact on climate and
956 biogeochemistry, Atmospheric Chemistry and Physics, 10, 10875-10893, 2010.
957 Mahowald, N. M., Lamarque, J. F., Tie, X. X., and Wolff, E.: Sea-salt aerosol response to climate
958 change: Last Glacial Maximum, preindustrial, and doubled carbon dioxide climates, Journal of
959 Geophysical Research-Atmospheres, 111, 2006a.
960 Mahowald, N. M., Muhs, D. R., Levis, S., Rasch, P. J., Yoshioka, M., Zender, C. S., and Luo, C.:
961 Change in atmospheric mineral aerosols in response to climate: Last glacial period, preindustrial,
962 modern, and doubled carbon dioxide climates, J. Geophys. Res., 111, D10202, 2006b.
963 Mahowald, N. M., Zender, C. S., Luo, C., Savoie, D., Torres, O., and del Corral, J.:
964 Understanding the 30-year Barbados desert dust record, Journal of Geophysical Research-
965 Atmospheres, 107, 4561, 2002.
966 Marticorena, B. and Bergametti, G.: Modeling the atmospheric dust cycle .1. Design of a soil-
967 derived emission scheme, Journal of Geophysical Research-Atmospheres, 100, 16415-16430,
968 1995.
969 Martin, J. H., Gordon, R. M., and Fitzwater, S. E.: The case for iron, Limnology and
970 Oceanography, 36, 1793-1802, 1991.
971 McKenna Neuman, C. and Nickling, W. G.: A theoretical and wind-tunnel investigation of the
972 effect of capillary water on the entrainment of sediment by wind, Canadian Journal of Soil
973 Science, 69, 79-96, 1989.

974   Menut, L., Perez, C., Haustein, K., Bessagnet, B., Prigent, C., and Alfaro, S.: Impact of surface
975   roughness and soil texture on mineral dust emission fluxes modeling, Journal of Geophysical
976   Research-Atmospheres, 118, 6505-6520, 2013.
977   Miller, R. L. and Tegen, I.: Climate response to soil dust aerosols, Journal of Climate, 11, 3247-
978   3267, 1998.
979   Mokhtari, M., Gomes, L., Tulet, P., and Rezoug, T.: Importance of the surface size distribution of
980   erodible material: an improvement on the Dust Entrainment And Deposition (DEAD) Model,
981   Geoscientific Model Development, 5, 581-598, 2012.
982   Neale, R. B., Chen, C.-C., Gettelman, A., Lauritzen, P. H., Park, S. U., Williamson, D. L.,
983   Conley, A. J., Garcia, R., Kinnison, D., Lamarque, J. F., D., M., Mills, M., Smith, A. K., Tilmes,
984   S., Vitt, F., Morrison, H., Cameron-Smith, P., Collins, W. D., Jacono, M. J., Easter, R. C., Ghan,
985   S. J., Liu, X., Rasch, P. J., and Taylor, M. A.: Description of the NCAR Community Atmosphere
986   Model (CAM 5.0), NCAR Technical Note, TN-486, pp. 268, 2010.
987   Oleson, K. W., Lawrence, D. M., Gordon, B. B., Flanner, M. G., Kluzek, E., Lawrence, P. J.,
988   Levis, S., Swenson, S. C., Thornton, P. E., Dai, A., Decker, M., Dickinson, R., Feddema, J.,
989   Heald, C. L., Hoffman, F., Lamarque, J.-F., Mahowald, N., Niu, G.-Y., Qian, T., Randerson, J.,
990   Running, S., Sakaguchi, K., Slater, A., Stockli, R., Wang, A., Yang, Z.-L., Zeng, Z., and Zeng,
991   X.: Technical Description of version 4.0 of the Community Land Model (CLM), 2010.
992   Perlwitz, J., Tegen, I., and Miller, R. L.: Interactive soil dust aerosol model in the GISS GCM 1.
993   Sensitivity of the soil dust cycle to radiative properties of soil dust aerosols, Journal of
994   Geophysical Research-Atmospheres, 106, 18167-18192, 2001.
995   Prospero, J. M.: Assessing the impact of advected African dust on air quality and health in the
996   eastern United States, Hum. Ecol. Risk Assess., 5, 471-479, 1999.
997   Prospero, J. M., Ginoux, P., Torres, O., Nicholson, S. E., and Gill, T. E.: Environmental
998   characterization of global sources of atmospheric soil dust identified with the Nimbus 7 Total
999   Ozone Mapping Spectrometer (TOMS) absorbing aerosol product, Reviews of Geophysics, 40,
1000   1002, 2002.
1001   Prospero, J. M. and Lamb, P. J.: African droughts and dust transport to the Caribbean: Climate
1002   change implications, Science, 302, 1024-1027, 2003.
1003   Prospero, J. M. and Nees, R. T.: Impact of the north african drought and el-nino on mineral dust
1004   in the barbados trade winds, Nature, 320, 735-738, 1986.
1005   Prospero, J. M., Uematsu, M., and Savoie, D. L.: Mineral aerosol transport to the Pacific Ocean.
1006   In: Chemical Oceanography, Riley, J. P. (Ed.), Academic Press, New York, 1989.
1007   Ravi, S., D'Odorico, P., Over, T. M., and Zobeck, T. M.: On the effect of air humidity on soil
1008   susceptibility to wind erosion: The case of air-dry soils, Geophysical Research Letters, 31, 2004.
1009   Ravi, S., Zobeck, T. M., Over, T. M., Okin, G. S., and D'Odorico, P.: On the effect of moisture
1010   bonding forces in air-dry soils on threshold friction velocity of wind erosion, Sedimentology, 53,
1011   597-609, 2006.
1012   Rea, D. K.: The paleoclimatic record provided by eolian deposition in the deep-sea - The
1013   geologic history of wind, Reviews of Geophysics, 32, 159-195, 1994.
1014   Ridley, D. A., Heald, C. L., and Prospero, J. M.: What controls the recent changes in African
1015   mineral dust aerosol across the Atlantic?, Atmospheric Chemistry and Physics, 14, 5735-5747,
1016   2014.
1017   Schepanski, K., Tegen, I., Todd, M. C., Heinold, B., Bonisch, G., Laurent, B., and Macke, A.:
1018   Meteorological processes forcing Saharan dust emission inferred from MSG-SEVIRI

29

1019 observations of subdaily dust source activation and numerical models, Journal of Geophysical
1020 Research-Atmospheres, 114, 2009.
1021 Shao, Y. P.: Physics and Modelling of Wind Erosion, Springer, Heidelberg, 2008.
1022 Solomon, S., Qin, D., Manning, M., Alley, R. B., Berntsen, T., Bindoff, Z., Chen, Z.,
1023 Chidthaisong, A., Gregory, J. M., Hegerl, G. C., Heimann, M., Hewitson, B., Hoskins, B. J.,
1024 Joos, F., Jouzel, J., Kattsov, V., Lohmann, U., Matsuno, T., Molina, M., Nicholls, N., Overpeck,
1025 J., Raga, G., Ramaswamy, V., Ren, J., Rusticucci, M., Somerville, R., Stocker, T. F., Whetton, P.,
1026 Wood, R. A., and Wratt, D.: Technical Summary. In: Climate Change 2007: The Physical Science
1027 Basis. Contribution of Working Group I to the Fourth Assessment Report of the
1028 Intergovernmental Panel on Climate Change Solomon, S., Qin, D., Manning, M., Chen, Z.,
1029 Marquis, M., Averyt, K. B., Tignor, M., and Miller, H. L. (Eds.), Cambridge University Press,
1030 Cambridge, United Kingdom and New York, NY, USA, 2007.
1031 Tegen, I., Harrison, S. P., Kohfeld, K., Prentice, I. C., Coe, M., and Heimann, M.: Impact of
1032 vegetation and preferential source areas on global dust aerosol: Results from a model study,
1033 Journal of Geophysical Research-Atmospheres, 107, 2002.
1034 Tegen, I., Werner, M., Harrison, S. P., and Kohfeld, K. E.: Relative importance of climate and
1035 land use in determining present and future global soil dust emission, Geophysical Research
1036 Letters, 31, 2004.
1037 Videen, G. and Chylek, P.: Scattering by a composite sphere with an absorbing inclusion and
1038 effective medium approximations, Optics Communications, 158, 1-6, 1998.
1039 Washington, R., Bouet, C., Cautenet, G., Mackenzie, E., Ashpole, I., Engelstaedter, S., Lizcano,
1040 G., Henderson, G. M., Schepanski, K., and Tegen, I.: Dust as a tipping element: The Bodele
1041 Depression, Chad, Proc. Natl. Acad. Sci. U. S. A., 106, 20564-20571, 2009.
1042 Werner, M., Tegen, I., Harrison, S. P., Kohfeld, K. E., Prentice, I. C., Balkanski, Y., Rodhe, H.,
1043 and Roelandt, C.: Seasonal and interannual variability of the mineral dust cycle under present
1044 and glacial climate conditions, Journal of Geophysical Research-Atmospheres, 107, 4744, 2002.
1045 Wilks, D. S.: Statistical Methods in the Amtospheric Sciences, Academic Press, Oxford, UK,
1046 2011.
1047 Zender, C. S., Bian, H. S., and Newman, D.: Mineral Dust Entrainment and Deposition (DEAD)
1048 model: Description and 1990s dust climatology, Journal of Geophysical Research-Atmospheres,
1049 108, 4416, 2003a.
1050 Zender, C. S., Newman, D., and Torres, O.: Spatial heterogeneity in aeolian erodibility: Uniform,
1051 topographic, geomorphic, and hydrologic hypotheses, Journal of Geophysical Research-
1052 Atmospheres, 108, 4543, 2003b.
1053 Zobeck, T. M.: Soil properties affecting wind erosion, Journal of Soil and Water Conservation,
1054 46, 112-118, 1991.
1055
1056
1057
1058